Spinal cord injury: What are the lesion effects on transplanted cells in an autograft model?

Authors:

Quentin Delarue[1,4]*, Matthis Brodier[1], Pauline Neveu[4], Laurine Moncomble[4], Alizée Hugede[1], Axelle Blondin[1], Amandine Robac[1], Clémence Raimond[4], Pamela Lecras[2], Gaëtan Riou[3], Nicolas Guérout[4]*.

Affiliations:

1. Normandie univ, UNIROUEN, UR3830 GRHVN, Institute for Research and Innovation in Biomedicine (IRIB), 76000 Rouen, France.

2. Normandie Univ, UNIROUEN, PRIMACEN Facility, IRIB, 76130 Mont-Saint Aignan, France & PBS-UMR6270 CNRS, FR3038 CNRS, 76130, Mont-Saint Aignan, France.

3. Normandie univ, UNIROUEN, INSERM U1234, CHU Rouen, Department of Immunology and Biotherapy, F-76000 Rouen, France.

4. Université Paris Cité, CNRS UMR8003, Saints-Pères Paris Institute for Neurosciences, F-75006 Paris, France.

***Corresponding Authors:**

Dr. Quentin Delarue: quentindelarue.rd@gmail.com

Pr. Nicolas Guérout: nicolas.guerout@u-paris.fr

Abstract:

Spinal cord injury (SCI) is a serious pathology of the central nervous system that result in loss of motor, sensory and autonomic functions below the level of the lesion and for which, unfortunately, there is currently no cure. In addition to the loss of function, SCI induces a systemic inflammation that is not confined to the spinal cord and whose effects are increasingly well characterized. In particular, SCI causes cerebral inflammation, which is responsible for the impairment of hippocampal and bulbar neurogenesis. Many therapies have been tested as potential treatments for SCI. In animal models, cell therapies have shown interesting effects such as medullary scar reduction, anti-inflammatory properties, axonal regrowth or neuronal survival, allowing better functional recovery. However, in human studies, their therapeutic capacities are less significant. Beyond obvious differences in pathophysiology and cell culture procedures, a key paradigm of cell transplantation differs between humans and animals. In animal models, transplanted cells are systematically taken from healthy animals, whereas in humans the immune incompatibility leads to the realization of autologous transplantation. Therefore, we were interested in the lesion effects on the neuro-repairing potential of olfactory ensheathing cells (OECs) harvested from olfactory bulbs.

Using functional sensory-motor studies, histological and gene expression analyses, we were able to demonstrate for the first time that the lesion negatively affects the therapeutic properties of cells used to treat SCI. These innovative results shed new light on the future use of cell transplantation in autologous transplantation after SCI.

INTRODUCTION:

Spinal cord injury (SCI) is a rare traumatic pathology of the spinal cord. It is caused by road or sports-related accidents, falls, or violence [1]. It is more common in young people and the over-60s, who are generally in good health [2]. Unfortunately, no curative treatment can be offered to people with SCI, so these patients remain disabled for life. Depending on the severity of the lesion SCI can result in complete or incomplete motor, sensory and/or autonomic deficits below the site of injury.

From a cellular and molecular point of view, the primary traumatic lesion is followed by a secondary lesion linked to the tissue reactivity. In particular, the initial damage induces blood vessel rupture, neuronal and oligodendrocyte cell death, which leads to neuronal dysfunction and immune cells infiltration such as neutrophils and macrophages, all of which increase the reactivity of resident immune cells, microglial cells, leading to the emergence of an inflammatory response [3,4]. The reactivity of these different immune cells induces a response from astrocytes, ependymal cells and pericytes, forming a spinal scar that prevents the lesion from spreading and secondary damages caused by inflammation [5–7]. The series of events following SCI has been well described and characterized in the spinal cord. However, it has been reported that SCI is also responsible for systemic inflammation [8]. The inflammatory state is also found in the brain, particularly in the hippocampus and olfactory bulb, leading to a decrease in neurogenesis and cognitive decline in mice and rat [9,10].

Many treatments have been investigated in experimental or clinical trials to provide a curative therapy for these patients. These treatments are based on different paradigms, including the modulation of the lesion environment by enzymes to increase axon regrowth or, more recently, methods using human-machine interfaces [11–13]. These therapeutic approaches include cell transplantation which is one of the most widely studied. Different cell types have been studied after SCI: stem cells such as hematopoietic or mesenchymal stem

cells [14,15] or differentiated cells such as Schwann cells [16] or olfactory ensheathing cells (OECs) [17]. Although cell types differ in origin and characteristics, identical regenerative mechanisms have been described in several studies. These cells have a therapeutic effect on SCI by modulating the spinal scar and reducing secondary damages [18].

Among cells studied, OECs are a very interesting therapeutic candidate. Their transplantation after SCI has shown anti-inflammatory and regenerative properties, allowing functional recovery in animal models. Indeed, these cells have been described to induce axonal survival and regrowth, but also to modulate the inflammatory response that occurs after SCI by acting on the polarization of microglia and macrophages, triggering a switch from a pro-inflammatory to an anti-inflammatory phenotype [19,20]. The properties of OECs and their ability to induce tissue repair and functional recovery after transplantation into SCI, without integrating into the spinal parenchyma, have led to their use in clinical trials. However, studies of bulbar OEC (bOEC) transplantation in humans have reported inconsistent results [21]. Indeed, some studies report an improvement of the ASIA score in treated patients while others show no difference after treatment.

Differences in culture, transplantation methods and physiopathology between humans and rodents may explain these different results. However, another important difference between animal and human studies is the transplantation paradigm. In humans, transplantation is autologous, meaning that cells come from the traumatized organism, whereas in animals, healthy animals are used for cell culture. The fact that many studies showed that SCI can induce systemic inflammation [10,22,23]; we are wondering if the lesion itself could affect neuro-regenerative properties of the transplanted cells. Therefore, in our study, we investigated the effects of SCI on bOECs properties in the context of transplantation for SCI treatment by mimicking an autologous transplantation model in mice.

MATERIALS AND METHODS

Animal care and use statement

The animal protocol was designed to minimize pain or discomfort to the animals. All experimental procedures were in accordance with the European Community guidelines on the care and use of animals (86/609/CEE; Official Journal of the European Communities no. L358; 18 December 1986), the French Decree no. 97/748 of 19 October 1987 (Journal Officiel de la République Française; 20 October 1987) and recommendations of the Cenomexa Ethics Committee (#26905).

Animals

Mice of either sex were group housed (two–five mice/cage, genders separated) in secure conventional rodent facilities on a 12-h light/dark cycle with constant access to food and water. A total of 270 mice were included in this study. We used three mouse lines in this study: 254 wild type (WT) C57BL/6 mice, 12 Rosa26-tdTomato mice and 4 (CAG-luc-GFP) L2G85Chco+/+ (FVB-Tg(CAG-luc,-GFP) L2G85Chco/J,) mice called Luciferase (LUX) thereafter. Then, LUX mice have been crossed with C57BL/6 mice three times consecutively to be sure to avoid any problem related to the strains. LUX mice were obtained from the Jackson Laboratory (https://www.jax.org/strain/008450, RRID:IMSR_JAX:008450).

All experiments were performed on adult mice aged 8-12 weeks (average weight 20 g for females and 25 g for males). All experimental groups were created with a sex ratio of 50:50. Our study consisted of four main experimental groups (Fig. 1):

Non-injured control group: animals without SCI used to define baselines for histological and functional experiments.

SCI group: animal received spinal cord injury without transplantation.

SCI + bOECs H group: animal received spinal cord injury and primary bOECs transplantation was performed immediately after SCI. Olfactory bulb (OB) used to prepare primary bOECs culture was obtained from uninjured animals.

SCI + bOECs I group: animal received spinal cord injury and primary bOECs transplantation was performed immediately after SCI. OB used to prepare primary bOECs culture was obtained from previously SCI injured animals.

Primary olfactory bulb culture and cell transplant preparation

Briefly, mice were anaesthetized with 2% isoflurane (Iso-Vet, Osalia, Paris, France), then euthanized by decapitation, and OBs were extracted from the brain and placed in cold phosphate buffered saline (PBS). After incubation in trypsin 0.25% (2.5% Trypsin 10X, 15090-046, Thermofisher), the tissue was mechanically dissociated. After dissociation, cells were cultured in T25 flasks with 5 ml DF-10S medium (DMEM:F12 + Glutamax, 0.5% penicillin/streptomycin and 10% heat-inactivated fetal bovine serum). One month after plating, cultures were trypsinized and cells were counted to prepare a cell suspension of 25,000 cells/µL in DF-10S for transplantation.

Flow cytometry and bOECs characterization

Cells were characterized by flow cytometry 1 month after plating. The number of primary bOECs were adjusted to a density of $2x10^5$ cells/ml PBS/ 0.5% bovine serum albumin (BSA) solution. TruStain FcX™ PLUS (BioLegend) was added to block non-specific binding. Cell populations were identified using anti-p75 nerve growth factor receptor (p75, Abcam, ab8874, RRID:AB_306827) and rat anti-platelet-derived growth factor β (PDGFRβ, Abcam, ab91066, RRID:AB_10563302) primary antibodies. OECs were identified as P75 positive and PDGFRβ negative cells. Stromal cells were identified as PDGFRβ positive and P75 negative cells. P75 and PDGFRβ primary antibody were revealed with the anti-rabbit phycoerythrin fluorochrome-conjugated (PE, poly4064, BioLegend, 406408,

RRID:AB_10643424) and the anti-rat Alexafluor 488 fluorochrome-conjugated antibodies (AF488, MRG2b-85, BioLegend, RRID:AB_2715913) respectively. Data were analyzed using FlowJo software (version 10.3; FlowJo LLC).

Real-time quantitative polymerase chain reaction characterization

Quantitative reverse transcription polymerase chain reaction (qRT-PCR) experiments were performed to evaluate the mRNA expression level of cytokines, chemokines and inflammatory molecules in OBs without SCI and 7 days after SCI and in BV2 cell cultures (BV2 control, BV2 + bOECs H conditioned medium (CM) and BV2 + bOECs I CM) (Table 1). In addition, qRT-PCR experiments were performed to measure mRNA expression levels of axon growth inhibitory and axon growth permissive molecules and neurotrophic factors in primary bOEC cultures (Table 2). Total RNA from bOECs was extracted after dissociation in the same manner as for the cultures, using Tri-reagent (Sigma) and Nucleospin RNAII Kit (Macherey-Nagel) according to the manufacturer's protocol. From each sample, 1.5 µg of total RNA was converted into single-stranded cDNA using the ImPromII reverse transcriptase kit (Promega) with random primers (0.5 µg/ml). Two ng of complementary DNA (cDNA) was amplified in the presence of 2X SYBR Green Mastermix (Applied Biosystems) containing preset concentrations of dNTPs, MgCl2 and forward and reverse primers using a QuantStudioTM 12KFlex (Applied Biosystems). Appropriate controls without reverse transcriptase or with H2O instead of cDNA were performed. Primers were designed using Primer Express software (Applied Biosystems) and validated by RT-PCR. The relative amount of cDNA in each sample was determined using the comparative quantification cycle (Cq) method and expressed as 2-DDCq. Three housekeeping genes were used to standardize the relative amount of cDNA: gapdh, b2m and actb. All experiments were performed in duplicate.

Surgical procedure and cell transplantation

SCI was performed at the T9-T10 level as previously described [19]. After dorsal incision and laminectomy of T7 vertebrae, incomplete spinal cord transection was performed to preserve the lower part of the ventral horns while completely damaging the central part and the dorsal horns of the spinal cord. The SCI was performed with a 25-gauge needle: cells were transplanted immediately after the lesion was created. bOECs were transplanted using a micromanipulator arm attached to a stereotactic frame (World Precision Instrument). Thus, bOECs were injected using a 1 mm sterile glass capillary needle attached to the micromanipulator. Injections were made at a depth of 1 mm, 1.5 mm from the midline, 5 mm rostral and caudal to the lesion site. Two injections of 2 µL containing 25,000 cells/µL of bOECs were delivered. Each injection was carefully administered within 1 minute. After surgery, the back muscles and skin were sutured and mice were checked daily, none of which showed skin lesions, infection or autophagy throughout the study.

BDA injection

For axonal growth analysis, mice received an injection of 2 µL biotinylated dextran amine (BDA, 0.2 g/ml, Thermo Fisher Scientific, D1956, Waltham, MA) diluted in PBS at the cervical level two days prior to euthanasia. BDA was injected using a 1 mm sterile glass capillary needle attached to the micromanipulator arm mounted on a stereotactic frame (World Precision Instrument). Injections were made at a depth of 1 mm, 1.5 mm from the midline. The injection was carefully delivered within 1 minute. After injection, the muscles and skin were sutured.

bOECs survival

The survival of LUX+/- bOECs was analyzed by bioluminescence using an *in vivo* XTREM 4XP spectrum cooled charge-coupled device optical macroscopic imaging system (Brucker). With intraperitoneal injections of D-luciferin (0.3 mg/g body weight,

XenoLightTM, Perkin Elmer), LUX+/- bOECs were monitored for three weeks and photon counts were measured as previously described using Brucker molecular imaging software. [24].

In addition to the bioluminescence experiments, the survival of bOECs was investigated using bOECs extracted from Rosa26-tdTomato mice. After transplantation into wild type mice, the intensity of Rosa26-tdTomato bOECs was analyzed by immunohistochemistry (see below).

Tissue preparation and sectioning

Thirty minutes before euthanasia, mice received analgesia (buprenorphine 0.17 mg/kg). Mice were then deeply anaesthetized with 5% isoflurane and given an intraperitoneal injection of sodium pentobarbital (100 mg/kg, euthoxin). Transcardial injections were made with cold PBS followed by cold 4% paraformaldehyde (PFA, Sigma Aldrich, 252549) in PBS. Dissected spinal cord and brain were post-fixed in 4% PFA overnight and cryoprotected in 30% sucrose (Life Technologies, Carlsbad, CA) for at least 48 hours. After embedding in Tissue-Tek OCT compound (Sakura, Tokyo, Japan), spinal cords were sectioned sagittally at 20 µm and brains sagittally at 30 µm. Sections were collected on slides and stored at -20°C until further use.

Immunohistochemistry

Identification of different cells and structures in spinal cord and brain was performed using primary antibodies diluted in PBS blocking solution containing 10% normal donkey serum (Jackson ImmunoResearch, Cambridge, UK) and 0.3% Triton-X100 (Sigma-Aldrich) to block non-specific fixation. Antibody incubation was performed overnight at room temperature in a humidified chamber. The following primary antibodies were used: Rabbit anti-platelet-derived growth factor β (PDGFRβ, Abcam, ab32570, RRID:AB_777165), mouse

anti-glial fibrillary acidic protein (GFAP Cy3-conjugated Sigma-Aldrich, C9205, RRID:AB_476889), rabbit anti-ionized calcium-binding adapter molecule 1 (Iba1, Wako, 019-19741, Osaka, Japan, RRID: AB_839504), rat anti-myelin basic protein (MBP, Millipore, MAB386, RRID:AB_94975), rabbit anti-laminin (Abcam, ab11575, RRID: AB_298179), goat anti-mMMR (CD206, R&D systems, AF2535, RRID:AB_2063012), rat anti-B-lymphocyte activation antigen B7-2 (CD86, Invitrogen, MA1-10299, RRID:AB_11152324), guinea pig anti-vesicular glutamate transporter 1 (vGlut1, Millipore, AB5905, RRID: AB_2301751) and Wisteria floribunda agglutinin biotin-conjugated lectin (WFA, Sigma, L1516, RRID: AB_2620171).

After washing, antibody staining was detected with species-specific fluorescence-conjugated secondary antibodies (Jackson ImmunoResearch). WFA antibody and BDA staining were visualized with Cy3-conjugated streptavidin (Jackson ImmunoResearch). Sections were counterstained with 4′,6-diamidino-2-phénylindole (DAPI; 1 μg/mL; Sigma-Aldrich) and cover slipped with Vectashield mounting medium (Vector Labs, Burlingame, UK).

Image acquisition analysis

The representative images for quantification of immunohistochemically stained areas for sagittal sections were taken using the Zeiss Apotome2 microscope setup and the Leica THUNDER Imager Tissue 3D microscope setup. For spinal cord analysis, the epicenter of the lesion was imaged using a 10x microscope objective. For brain analysis, bulb images were taken using 20x microscope objective. Image processing and assembly was performed using ImageJ software.

Quantification of immunohistochemically stained areas

Three to five sections per animal were examined to determine the epicenter of the lesion. An image of the epicenter was then taken and analyzed. On these sagittal sections, GFAP negative (-), PDGFrβ positive (+), MBP- and Laminin+ areas were measured. NeuN+, WFA+, Iba1+, CD86+, CD206+, Iba1+/IL1β+, Iba1+/IL4+ cells and BDA+/vGlut1+ axons were counted after standardization of the area considered with a rectangle of 1000 µm x 1000 µm.

Primary OB conditioned-medium preparation

Primary OB cultures from uninjured and injured mice were prepared as described above. Four weeks after plating, the cultures were washed twice with PBS. The medium was then changed and CM was obtained 4 days later. The CM was placed in Amicon Ultra-15 3K ultrafiltration tubes (Millipore) and centrifuged at 5000g for 1 h at room temperature to concentrate it. From an initial volume of 6 mL, approximately 1 mL of concentrated CM was obtained by ultrafiltration. The CM was immediately stored at -80°C for preservation.

BV2 Cell line cultures

The BV2 cell line was obtained from ATCC (EOC CRL-2467TM). Cells were first thawed gently in a water bath at 37°C. Cells were then cultured in T25 flasks containing DMEM high glucose (GIBCO), 20% fetal bovine serum (FBS), 0.5% penicillin/streptomycin for the first 48 hours. After this initial culture, a first passage was performed. To pass cells, the medium was removed and cells were washed twice with PBS. After adding 5 mL of trypsin EDTA, the flasks were placed in the incubator for 10 minutes. To inhibit trypsin, culture medium containing FBS was added. After centrifugation at 500g for 5 minutes, cells were resuspended in 1 mL of culture medium. The culture medium then consisted of DMEM glutaMAX high glucose (GIBCO), 10% FBS and 0.5% penicillin/streptomycin. One week after plating, cultures were passed, re-plated and divided into three experimental groups: 1 - BV2 control, 2 - BV2 + bOECs H CM and 3 - BV2 + bOECs I CM. Cells from these 3 groups

were cultured for 3 days. Cultures were then trypsinized and immediately stored at -80°C for preservation for qRT-PCR analysis.

Locotronic test: Foot misplacement apparatus

Experiments were performed as previously described by Chort et al. (Intellibio, Nancy, France) [25]. The apparatus consists of a flat ladder on which the animal can move from the start zone to the arrival zone. On both sides of the ladder, infrared sensors allow the visualization and recording of the animal's movements. The location and precise length of time of all errors are recorded, in distinguishing errors from forelimb, hindlimb, and tail. Based on all recorded data, the number of hindlimb errors, total hindlimb error time and total crossing time were provided by the software and compared between groups of animals (Fig. 4B).

All mice were pre-trained on the ladder, three times 1 week prior to injury. Experiments were performed three times 14, 28 and 56 days after SCI for the bOECs transplanted groups.

Hargreaves

A Hargreaves plantar test (Ugo basile®) was performed as previously described by [26]. Briefly, after isolation for 5 min, a radiant heat source was applied to the plantar surface of the hindpaw. The time between the onset of the thermal radiation stimulus and the onset of paw withdrawal was measured by computer. The time of paw withdrawal was defined as the hindpaw withdrawal latency. Experiments were performed 14, 28 and 56 days after SCI for the bOECs transplanted groups.

CatWalk XT automated gait analysis

Motor coordination was performed and analyzed using the CatWalk XT automated system (Noldus; RRID:SCR_004074) [27]. In a dark room, mice were placed on the walkway and allowed to walk from one end to the other. The floor of the walkway consisted of a glass surface that transformed footprints of mice into light reflections in the form of illuminated footprints. The light reflection was recorded by a camera positioned under the walkway, the footprint image was converted into a digital signature and processed using CatWalk XT 9.1 software with a minimum threshold set at 80 (a.u. ranging from 0 to 225). After identification and labelling of footprints, data on static and dynamic gait parameters were generated from 3 consecutive trials (Fig. 4L and O). The average data of these parameters were analyzed and compared between experimental groups. If mice stopped halfway across or turned around during the run, the recording was stopped and the run was restarted to obtain 3 good crossings from one end to the other. Experiments were performed 56 days after SCI.

Statistical analysis

All data are presented as average ± standard deviation (SD). All statistical analyses were performed using the GraphPad Prism program, version for windows (GraphPad Software; 8.0.1.244).

In the figure comparing two groups, the comparison of average was performed using the two-way Mann-Whitney test. In the figure comparing three groups, comparison of medians was performed using the two-way Kruskal-Wallis test followed by Dunn's post-test. Statistical analysis in each assay is detailed in the figure legends. A p-value < 0.05 was considered statistically significant.

RESULTS

SCI alters gene expression in olfactory bulbs tissue and primary bOEC cultures

To investigate the effects of the SCI on distant tissues that could be used for autograft transplantation, we assessed the effects of SCI, 7 days after the lesion, on OB tissue and primary OB cultures by immunohistology, qRT-PCR and flow cytometry experiments (Fig. 2). A chronology of microglial cell reactivity in the OB was performed using immunohistology (Fig. 2A-D). Quantification of the total number of Iba1+ cells (Fig. 2A and B), the total number of double positive Iba1+/CD86+ cells (Fig. 2A and C) and the percentage of CD86+/Iba1+ cells among the Iba1+ cells (Fig. 2A and D) were assessed without SCI and at 3, 6, 12, 24, 48 hours and 7 days after injury. Our results show that the total number of Iba1+ cells does not change over time after SCI compared to the uninjured condition (Fig. 2B). On the contrary, the total number of double positive Iba1+/CD86+ cell is increased at 2 and 7 days after SCI compared to uninjured animals (Fig. 2C). Finally, our analyses indicate that the percentage of CD86+/Iba1+ cells among the Iba1+ cells is increased at 3 h after SCI, decreases to the control (No SCI) level at 12 h after SCI, and increases a second time at 7 days after SCI in comparison to uninjured and to 12 h after SCI conditions (Fig. 2D).

Therefore, the effect of SCI on bOEC primary cultures was investigated (Fig. 2E-G). First, the composition of bOEC primary cultures was measured by flow cytometry. These analyses show that SCI modifies the ratio between OECs (p75-positive cells) and fibroblasts (PDGFrβ-positive cells) when cells are plated 14 days after SCI, but not at 7 days after SCI (Fig. 2F). qRT-PCR experiments were then performed on bOEC primary cultures 7 days after SCI and compared with bOEC primary cultures obtained from uninjured animals (Fig. 2G). Results show that SCI modulates the expression of genes involved in extracellular matrix (ECM) production and axonal plasticity processes, such as *sema3f*, *neo1*, *ntn1* or *lgals1*. In addition, SCI changes the expression of immunomodulatory genes (*il6* and *tnf-a*) and growth

factor genes (e.g. *bdnf* or *vegfb*) in particular genes involved in scar-forming molecules such as *ctgf*, *fgf1* or *tgfβ2* or *tgfβ3* (Fig. 2G).

The survival of bOECs I mice is identical to that of bOECs H after transplantation

To clarify whether the initial injury modulates the survival of bOECs after transplantation, bioluminescence and tdTomato positive bOEC transplantation experiments were performed up to 28 days after SCI (Fig. 3). Bioluminescence experiments show that in both transplanted groups (bOECs H and bOECs I) any surviving cells could be observed 21 days after SCI (Fig. 3A and B). These experiments also reveal that there is no difference between the two groups 7 and 14 days after SCI (Fig. 3A and B). To confirm these results, tdTomato positive bOECs were transplanted and immunohistological analyses were performed 14, 21 and 28 days after SCI (Fig. 3C and D). Measurements of tdTomato positive intensity show that there is no difference between the two groups 14, 21 and 28 days after SCI (Fig. 3C and D).

Therapeutic capacity induced by bOEC transplantation is less important when bOECs are obtained from SCI mice.

To assess whether the changes expressed at the RNA level in primary cultures of bOECs affect the neuroregenerative capacity of these cells after transplantation in the context of SCI, we evaluated functional recovery (Fig. 4A). First, the Locotronic test (Fig. 4B) was performed in the SCI, SCI + bOECs H and SCI + bOECs I groups 14, 28 and 56 days after SCI (Fig. 4C-K). In addition, fine motor movements were assessed using a CatWalk test at 56 days post SCI (Fig. 4L-O). Our analyses show that when bOECs are obtained from injured mice (bOECs I), their transplantation does not improve the number of hindlimb errors (Fig. 4C, F and I) at 14, 28 and 56 days after SCI, and only slightly improves the other parameters. In fact, except for the total hindlimb error time 14 days after SCI (Fig. 4D) and the time

needed to cross the corridor 28 days after SCI (Fig. 4H), the Locotronic test reveals that the bOECs I group is comparable to the SCI group.

To confirm these results, CatWalk experiments were performed 56 days after SCI. The results obtained show that the base of support (BOS) (Fig. 4M) is increased in bOECs I compared to bOECs H mice, also the stride length tends to be reduced in the bOECs I group compared to bOECs H (Fig. 4N).

The Locotronic test and CatWalk analyses indicate that the improvement in both static and dynamic parameters is lost in bOECs I group compared to the bOECs H group. To correlate the results with functional recovery, immunohistological analyses were performed 14, 28 and 56 days after SCI (Fig. 5). Spinal scar and demyelination were assessed by quantification of fibrotic (Fig. 5B, F, J and M) and glial scar (Fig. 5C, G, K and N) and quantification of demyelinated areas (Fig. 5D, H, L and O) over time. As previously described, bOEC H transplantation modulates the lesion scar by decreasing the fibrotic scar (PDGFrβ+ area) and demyelination (MBP- area) after SCI and by increasing the glial scar (GFAP- area) 14 and 56 days after SCI (Fig. 5A, B, C, D, I, J, K and L), with the same tendency without statistical difference 28 days after SCI (Fig. 5E-H) [28]. More interestingly, immunohistological results show that bOEC I transplantation does not modulate fibrotic and glial scars 14 (Fig. A-C), 28 (Fig. E-G) and 56 days (Fig. I-K) post SCI. Analysis of the demyelination process shows that bOEC I transplantation reduces the MBP negative area only at 56 days post SCI, but not at 14 and 28 days post SCI (Fig. 5L, D and H respectively). The time course of SCI shows that at 14 and 28 days post SCI, the spinal cord scar is larger in animals that had received a bOEC I graft. By 56 days post SCI, the scar size tends to be identical to that of animals who had received bOECs H (Fig. M-O).

Collectively, our results demonstrate that the initial trauma induced prior to primary culture of bOECs alters their ability to promote functional recovery and tissue repair after SCI and transplantation.

Transplantation of bOECs induces axonal regrowth, but this regrowth is associated with synaptogenesis and pain-related behavior only in mice that received bOECs from healthy mice.

It has been previously described that cell transplantation, including transplantation of OECs, can induce allodynia after SCI [29]. To investigate this, the Hargreaves plantar test was performed 14, 28 and 56 days after SCI (Fig. 6A and B). In addition, hindpaw pressure was assessed using the CatWalk system 58 days after SCI (Fig. 6A, C and D). As previously described, bOEC H transplantation reduces hindpaw withdrawal time 14 days after SCI compared to SCI mice (Fig. 6B). Experiments also demonstrate that bOECs I transplanted animals had a hindpaw withdrawal time comparable to the SCI group, which was also increased compared to the bOECs H group 14 and 56 days after SCI (Fig. 6B). To confirm these results, the hindpaw pressure of the hindlimbs was measured 56 days after SCI. Measurements show that maximum and mean hindpaw pressures tend to decrease in bOECs H mice compared to bOECs I mice (Fig. 6C and D), which may indicate pain-related behavior during locomotion in bOECs H mice.

Previous studies have described that pain-related behavior can be associated with axonal regrowth and formation of new synapses [30]. The composition of the ECM plays a crucial role in axonal regrowth or axonal inhibitory processes as well as synaptogenesis. Therefore, the presence of laminin (Fig. 6A, E and F), an ECM molecule permissive for axonal growth, was examined. As the size of the laminin area is related to the size of the lesion core (PDGFβ+ area), we measured the ratio of laminin+ area to PDGFβ+ area. It appears that the relative size of the laminin+ area is increased in both transplanted groups

compared to SCI group 14 days after SCI and only in the bOECs H group compared to the SCI and bOECs I groups 28 and 56 days after SCI (Fig. 6E and F).

To investigate axonal regrowth and the formation of new synapses, BDA anterograde tracing experiments (Fig. 6A, G, I, J and K) and colocalization analysis of BDA and VGlut1 staining (Fig. 6A H and L) were performed. As previously described [31], measurement of the number of BDA-positive axons present in the lesion core shows that bOEC transplantation induces modest axonal regrowth after SCI compared to the SCI group (Fig. 6I-K). Indeed, our results indicate that bOECs I mice show an increase in the number of BDA+ fibers in the lesion core 14 days after SCI, whereas bOECs H induces it 28 days after SCI (Fig. 6I and J respectively). Fifty-eight days after SCI, no difference is observed between groups (Fig. 6K). In addition, colocalization analysis of BDA and VGlut1 staining was performed 14, 28 and 56 days after SCI (Fig. 6A, H and L). This analysis shows that bOEC H transplantation increases synaptogenesis at the rostral part of the spinal cord compared to SCI groups and at the lesion core 28 days after SCI compared to the SCI group and bOECs I group (Fig. 6L). Fifty-six days after SCI, bOEC H transplantation also enhances synaptogenesis at the rostral part of the spinal cord compared to the SCI group and at the lesion core compared to bOECs I group and to the SCI group (Fig. 6L). In contrast, bOEC I transplantation did not modulate synaptogenesis, except at 14 days after SCI, where bOEC I transplantation increased it at the caudal part of the spinal cord compared to the SCI group (Fig. 6L). These results tend to demonstrate that bOEC H transplantation induces a more supportive microenvironment for axonal regrowth.

Taken together, our results indicate that bOEC H transplantation modifies the lesion scar ECM, which enhances axonal regrowth and synaptogenesis, and that bOEC I transplantation plays a weaker role on these parameters.

Transplantation of bOECs from injured animals fails to improve neuronal survival.

Neuronal survival was assessed in the three groups 14, 28 and 56 days after SCI (Fig. 7A, B, C, D, G and J). NeuN+ cells were counted at the rostral, caudal and lesion core of the spinal cord. As described in the literature, bOEC H transplantation increases neuronal survival. [32]. Indeed, our results show that 14 days after SCI, neuronal survival is increased in bOECs H animals at the rostral part of the spinal cord compared to SCI group (Fig. 7D). Twenty-eight days after SCI, bOEC H transplantation increases the number of NeuN+ cells in both rostral and caudal parts of the spinal cord compared to SCI animals (Fig. 7G). Finally, 56 days after SCI, results show that there is no difference between the groups (Fig. 7J). These analyses demonstrate that bOEC I transplantation does not improve neuronal survival 14, 28 and 56 days after SCI.

We then measured the number of NeuN+/WFA+ cells at rostral and caudal parts and at the lesion core of the spinal cord 14, 28 and 56 days after SCI. Fourteen days after SCI, the number of NeuN+/WFA+ cells is increased in the bOECs H group at the lesion core compared to the SCI group (Fig. 7E), with no difference between groups 28 days after SCI (Fig. 7H). Interestingly, at 56 days post SCI, our results indicate that the number of NeuN+/WFA+ cells is increased in bOECs H group compared to the SCI group at the lesion core, whereas the number of NeuN+/WFA+ cells is increased in the rostral and caudal parts of the spinal cord in bOECs I animals compared to the SCI group (Fig. 7K).

In addition to quantifying the number of NeuN+/WFA+ cells, WFA intensity was also assessed at 14, 28 and 56 days after SCI at the rostral and caudal parts and at the lesion core of the spinal cord (Fig. 7F, I and L). Fourteen days after SCI, bOEC transplantation improves WFA intensity quantifications at rostral and caudal parts and at the lesion core with a tendency for bOECs I group compared to SCI group and with significant differences for bOECs H group (Fig. 7F). At 28 days after SCI, quantification of WFA intensity shows that bOEC H transplantation increases this parameter at the lesion core compared to the SCI

group, with no difference between groups at 56 days after SCI (Fig. 7I and L respectively). At these time points, no difference is observed between SCI + bOECs I group and SCI group (Fig. 7I and L).

Transplantation of bOECs modulates the inflammatory microenvironment after SCI with moderate effects when bOECs are obtained from injured mice.

The immunomodulatory role of OECs after transplantation has recently been highlighted in several studies (Jiang et al., 2022). Therefore, we investigated immunomodulatory properties of bOEC H and bOEC I transplantation at 14, 28 and 56 days after SCI (Fig. 8). First, the number of Iba1+ cells present at rostral and caudal parts of the spinal cord and in the lesion core was measured. This analysis shows that there is no difference between the groups overtime (Fig. 8A). Macrophages and microglial cells can express anti-inflammatory or pro-inflammatory profiles with the respective expression of CD206 and CD86 markers. The ratio of CD86+/Iba1+ and CD206+/Iba1+ cells were assessed 14, 28 and 56 days after SCI at rostral and caudal parts of the spinal cord and in the lesion core (Fig. 8B-I). Fourteen days after SCI, bOEC H transplantation decreased the ratio of CD86+/Iba1+ cells at rostral part of the spinal cord and increased the ratio of CD206+/Iba1+ cells at rostral and caudal parts of the spinal cord compared to SCI animals. Transplantation of bOECs I tends to change the profile of microglia/macrophages in the same way at this time point, with no significant difference compared to the SCI group (Fig. 8D and E). Twenty-eight days after SCI, both bOECs transplanted groups modulate the microglia/macrophage profile (Fig. 8F and G).

Indeed, the ratio of CD86+/Iba1+ cells is reduced at the lesion core and at the caudal part of the spinal cord in both transplanted groups compared to the SCI animals and is also reduced at the rostral part of the spinal cord in the bOECs H group (Fig. 8F). The analysis also reveals that the ratio of CD206+/Iba1+ cells is increased in both transplanted groups at

rostral and caudal parts of the spinal cord compared to the SCI group, with a significant difference only between the bOECs H and SCI groups (Fig. 8G). Interestingly, 56 days after SCI, bOEC I transplantation increased the ratio of CD86+/Iba1+ cells at rostral and caudal part and lesion core of the spinal cord compared to bOECs H animals (Fig. 8H). Furthermore, the ratio of CD86+/Iba1+ cells at the lesion core is also increased between bOECs I and SCI groups. No difference is observed in CD206+/Iba1+ ratio analyses between groups (Fig. 8L).

To complete the analysis of bOECs properties in modulating inflammation, we performed qRT-PCR analyses on BV2 cell cultures (microglial cell line) exposed to conditioned media obtained from bOEC H (BV2 + bOECs H medium) and bOEC I (BV2 + bOECs I medium) cultures (Fig. 8J). The results obtained show that chemoattractant (*ccl5*) or inflammation activator genes (e.g. *csf1* or *cx3cr1*) are upregulated in BV2 + bOECs I compared to BV2 + bOECs H (Fig. 8K). It also appears that pro-inflammatory genes (e.g. *il1b*, *cxcr4*, *ifngr2*) are upregulated in BV2 + bOECs I compared to BV2 + bOECs H and anti-inflammatory genes are downregulated (*il10ra*). The comparison between BV2 and BV2 + bOECs H shows that activated stage (*p2ry12* and *p2rx4*) and pro-inflammatory (*ccl5* and *cx3cr1*) genes are downregulated and pro-remyelinating (*ccr5*) gene is upregulated in BV2 + bOECs H (Fig. 8L). Whereas pro-inflammatory genes (e.g. *ccl4* or *cxcr4*) are upregulated in BV2 + bOECs I compared to BV2 (Fig. 8M).

Collectively, our results demonstrate that the initial injury modulates bOECs I CM, which in turn alters gene expression of BV2 cell lines *in vitro*. Interestingly, these effects found *in vitro* do not strongly modify the *in vivo* properties of bOECs after transplantation in the context of SCI.

DISCUSSION

Spinal cord injury and regeneration by bOEC transplantation

The main purpose of our study was to investigate SCI consequences on brain and peripheral tissues. In particular, on the impairment of cell therapeutic capacities that could be used in an autograft context. Cellular responses and tissue remodeling that occur after SCI are well described in spinal tissue but only few studies have investigated the cellular responses induced by the trauma in the whole body. SCI is characterized by neuronal, glial, microglial and peripheral immune cells activation. Immune cells induce the formation of an inflammatory reactive environment causing cell death which in turn is responsible for the spread of neurological deficits and the functional losses but which also leads to formation of the spinal scar and triggers regenerative mechanisms [33]. Axonal regrowth and restoration of functional network are challenged by the limited plasticity of the spinal cord due to a dense fibrotic scar and an environment rich in pro-inflammatory cytokines, myelin fragments, chondroitin sulfate proteoglycans (CSPGs), damage-associated molecular patterns (DAMPs) and other inhibitory molecules [5,34]. Conversely, axonal regrowth and synaptic reestablishment need the presence and the secretion of anti-inflammatory cytokines, growth factors and permissive molecules supplied at least partly supplied by ependymal cells [35,36]. Neuronal survival and connectivity are also modulated by the perineuronal net (PNN). Indeed, at early stage (14 days after SCI), this structure, which surrounds the soma of neurons and their dendritic processes, provides protection against inflammation and apoptosis-induced molecules. Then, at later stage (56 days after SCI), it is gradually degraded, mediated by microglial cells, to allow new synaptic connections [37,38].

The inflammatory response is not limited to the spinal cord. Days following injury, cytokines and chemokines are detectable in rodent and human serum [8], and consequences associated with peripheral immune cell activation are present in other organs such as the spleen [39], kidneys, lungs [40], liver [41], adipose tissue [42] and brain [43]. For example,

SCI is associated with brain inflammation and cognitive deficits, particularly in the olfactory bulbs, cortex, thalamus and hippocampus. Recent studies report that the spread of inflammation is due to the presence of cytokines and immune cells into cerebrospinal fluid after SCI [44].

Therefore, we asked whether SCI could impair the known effects of cell therapy: bOEC transplantation. The bOEC transplantation effects are well described in several species including dogs, cats, rodents and non-human primates after SCI as well as in humans [45]. After SCI, bOEC transplantation improves functional recovery by modulating of spinal scar composition, both from a cellular and molecular levels. Analyses of molecules secreted by bOECs show their ability to produce *in vitro* and *in vivo*, growth factors, ECM modulating molecules and axonal regrowth facilitating molecules [45]. When transplanted after SCI, bOECs participate in neuroprotection, limiting secondary injury and improving the preservation of axonal networks spared by primary damages [32]. Through metalloproteinase secretion, bOECs degrade the axonal inhibitory ECM, in particular CSPGs present in the spinal scar and stimulate the production of axonal regrowth permissive molecules [28,46,47]. They also modulate microglial/macrophages activation through direct communication, through the release of cytokines and chemokines and by indirect effects in sparing spinal cord tissue. They help to reduce microglial/macrophages activation, allowing permissive tissue for neuronal network regeneration [48]. Overall, combined effects of bOEC transplantation lead to improve spinal cord plasticity allowing axonal regrowth, myelination and stabilization of neuronal networks favoring functional recovery [49].

However, it has also been reported that cell transplantation can induce pain-related behavior such as allodynia [29]. This can be explained by the release of growth factors that stimulate neuronal survival and by the enhancement of axonal regrowth. Moreover, it can be due to an overactivity of the preserved axons, induced by the cellular environment and

possibly by an increase in plasticity [50]. Indeed, to reconstitute neuronal networks, PNN surrounding neurons must be modulated over time to allow synaptic connections. It has recently been reported that reduction of PNN contributes to neuronal overactivity which in turn induces pain [51].

Here, our results provide new information on the mechanisms induced by bOEC transplantation after SCI. Indeed, we show that bOEC transplantation promotes the formation of axon permissive spinal scar by enhancing laminin deposition (Fig. 6E-F). In addition, to its effects on spinal scar, bOEC transplantation favors axonal regrowth and axon sprouting into the lesion core (Fig. 6I and J). Furthermore, our results demonstrate also that bOEC transplantation improves synaptic connectivity, objectified by VGlut1+/BDA+ co-staining, at the chronic stage (56 days after spinal cord injury), at rostral part of the spinal cord and at the lesion core (Fig. 6L). Interestingly, results regarding synaptic formation do not correlate with a decrease of PNN density at later stage (Fig. 7H, I, K and L). Nevertheless, we can observe that the PNN is preserved and increased at early stage after transplantation compared to untreated injured mice (Fig. 7F). We can hypothesize that, preservation of PNN protects neurons and increases their survival during the acute phase and the beginning of the chronic phase (28 days after SCI) (Fig. 7D and G). Altogether, bOECs abilities contribute to the regeneration of axonal networks and the formation of new synapses, both improving functional motor recovery (Fig. 4), but are also responsible of pain related thermal stimuli (Fig. 6A). It is important to note, that the identification of an increase in the number of synapses does not indicate that the network is functional. Electrophysiological analyses would allow us to highlight the functionality of synapses by examining neuronal connectivity between the neuron and its target.

Altogether, our results confirm the known effects of bOEC transplantation previously described in other studies, regarding expression of molecules modulating spinal scar and

axonal regeneration. Moreover, here we described the main role played by OECs on microglia/macrophages reactivity and polarization. In effect, our results show that bOEC transplantation can modulate the ratio of proinflammatory (CD86+) and anti-inflammatory (CD206+) microglia/macrophages present into the lesion site. We have also deepened the knowledge about bOECs effects on modulation of the PNN, which can, at least in part, explain the increase of painful sensitivity observed in bOECs H group.

Therapeutic effects of bOEC transplantation are impaired by spinal cord injury in an autograft model

To determine whether SCI can modulate therapeutic effects of cells in autologous transplantation paradigm, we have transplanted bOECs, obtained from spinal cord injured mice and collected seven days after the lesion, in other spinal cord injured mice. Our findings demonstrate for the first time that the initial trauma reduces therapeutic effects of bOECs. In fact, bOEC (from injured mice) transplantation, shows no significant difference in terms of functional recovery compared to SCI (untreated animals) and bOECs H (bOECs obtained from uninjured mice) groups. On the contrary, it shows a trend with an intermediate effect and a high heterogeneity in functional performances (Fig. 4C-K), as well as in hindpaw placements during locomotion (Fig. 4M and N). This potential difference in term of neuroregenerative properties was confirmed by the assessment of spinal scar composition. Indeed, transplantation of bOECs I does not change the composition of the spinal scar compared to untreated mice. While bOEC H transplantation reduces the overall size of the fibrotic scar and thus reduces the area without astrocytes, bOEC I transplantation fails to do the same (Fig. 5B, C, F, G, J and K). Analyses of the demyelinated areas also show that bOEC H transplantation reduces MBP negative areas 14 and 56 days after SCI whereas bOEC I transplantation do not reduce it 14 and 28 days after SCI but could only decrease it 56 days after SCI (Fig. 5D, H and L respectively).

Thus, we hypothesized that the modulation of the spinal scar may be related to differences between bOECs H and bOECs I survival after SCI and transplantation. Our results show that the survival of bOECs H and I after transplantation are identical. In fact, 4 weeks after SCI, based on two different approaches, we could not find any surviving cells in the spinal cord in either group of bOECs transplanted (Fig. 3). These results are of primary importance because they show that the differences observed after bOEC H and bOEC I transplantation are not due to an effect on cell survival but are mainly due to intrinsic differences between cells *per se*.

To confirm this hypothesis, we examined the effects of bOEC I transplantation on laminin deposition, axonal regrowth and synapse formation. Our results show that, overall bOEC I transplantation decreases laminin deposition compared to bOEC H transplantation (Fig. 6E and F), has limited effects on axonal regeneration resulting in a decrease of vGlut1 synapse formation without major influences on axonal sprouting (Fig. 6I-L). In addition, to these experiments, neuronal survival and PNN were assessed after bOEC I transplantation. It appears that bOEC I transplantation does not significantly improve neuronal survival after SCI compared to untreated animals whereas bOEC H transplantation improves it 14 and 28 days after SCI (Fig. 7 A, B, C, D, G and J). More interestingly, WFA analysis shows that bOEC I transplantation enhances the ratio of WFA+/NeuN+ neurons 56 days after SCI (Fig. 7K). As described above, it has been reported that PNN degradation is a necessary process after injury to induce neuronal plasticity and the establishment of synaptic connections at the chronic stage [38], which may be related to the fact that bOEC I transplantation fails to enhance formation of new synapses 56 days after SCI (Figure 6L).

These results could be explained by the differences in gene expression observed between bOEC H and bOEC I primary cultures in our qRT-PCR experiments (Fig. 2G). In fact, bOEC I primary cultures overexpresses genes involved in scar forming molecules, such

as *ctgf*, *fgf1* or *tgfβ2* or *3*, which stimulate proliferation of stromal cells and type A pericytes and also increase ECM deposition by astrocytes, leading to an increase in the formation of the fibrotic scar. This analysis also demonstrate that other gene expressions are modulated in bOEC I primary cultures. Indeed, a set of genes implicated in ECM modulation and axonal plasticity is upregulated as *sema3f*, *neo1*, *ntn1* or *lgals1* (Fig. 2G) which are known to negatively influence axonal regrowth.

Altogether, these results suggest that the gene expression changes observed in bOEC I primary cultures directly affect spinal scar formation, neuronal survival and axonal regrowth and reduce the therapeutic efficacy of these cells.

As described above, microglia/macrophage populations are important players in spinal cord regeneration. The number and polarization of these cells have a strong influence on spinal tissue scarring and axonal regeneration [52]. We found that *in vitro*, microglial cell cultures (BV2 cell line) are modulated by the molecules secreted by bOECs, and in particular by the CM of bOEC I primary cultures. In fact, BV2 cultured with bOECs I concentrated medium, overexpress genes encoding cytokines, chemokines, trophic factors and cellular receptors. Among these modulated genes, most of them are involved in microglial activation (e.g., *csf1*, *cx3cr1*, *p2rx4*, *p2r12*) and in polarization towards a pro-inflammatory phenotype (e.g., *ccl5*, *il1β*, *cxcr4*, *ifngr2*), while genes expression of BV2 cultured with bOECs H concentrated medium is closer to the gene expression of BV2 control cultures (without conditioned medium) (Fig. 8K). BV2 cultured with bOECs H concentrated medium down regulate the expression of proinflammatory genes compared to BV2 control while at the same time BV2 bOECs I upregulate their expression of proinflammatory genes compared to control (Fig. 8L and M). These results can be linked to the increase in *il1β* and *tnf-α* gene expression observed in bOECs I primary culture in our qRT-PCR experiments (Fig. 2G). At the opposite, *in vivo* analyses, show that there is no major difference in microglia/macrophage activation

and polarization between bOECs H and bOEC I transplantation at the early stage and at the beginning of the chronic stage after SCI (Fig. 8A-G). Nevertheless, it can be noted that only the bOECs H group shows a significant increase in the percentage of pro-regenerative/anti-inflammatory microglia/macrophages, identified by CD206, in the rostral and caudal parts of the spinal cord compared to SCI mice at these stages. On the other hand, at the chronic stage, the time of the second microglia/macrophage wave, the percentage of pro-inflammatory microglia/macrophages is reduced after bOEC H transplantation compared to bOEC I transplantation (Fig. 8H). These results may indicate that bOECs H in the chronic stage, create a less reactive extracellular environment that favors axonal network regeneration by facilitating mechanisms involved in PNN degradation and synaptic connection formation (Fig. 6L and 7K).

Altogether, our results demonstrate for the first time the major impact of the initial injury on the therapeutic effects of cells that can be used for cellular transplantation after SCI. It also highlights one of the reasons that may explain the differences observed in spinal cord regeneration and functional recovery after cellular transplantation in mice and humans. Indeed, the initial physical trauma does not only lead to localized disturbances at the site of the injury [41]. The whole body is in an "inflammatory state" in response to circulating cytokines, chemokines and immune cells, causing intrinsic changes in the cells used for autografting that are responsible for their reduced therapeutic efficacy. The inflammatory response that occurs after SCI is the main actor in the propagation of trauma. The use of anti-inflammatory drugs to reduce inflammation in the first hours, days and weeks after SCI, in order to reduce the cellular response and increase the therapeutic effect of autologous cells, may have adverse effects. Indeed, it has been shown that the immune response, and in particular the microglial/macrophage response, is important for tissue regeneration after SCI. The use of anti-inflammatory drugs has been shown to worsen spinal scar size, reduce axonal

regeneration and limit functional recovery [53,54]. In our study, we chose to collect the olfactory bulbs 7 days after SCI, at early stage. One solution would be to collect cells several weeks or months after SCI when immune response is lower, but it is important to consider the chronology of the physiopathology. It has been described, at least in animal studies, that the most effective therapeutic window is at early stage after SCI. Indeed, the use of an effective therapy at early stage should make it possible to reduce axonal and, more broadly, tissue damages and limit the exacerbation of the inflammatory response.

Conclusion

Finally, our results should be put into a clinical perspective. Indeed, autograft transplantation is envisaged as potential treatment to cure SCI. However, our results demonstrate for the first time that traumatic SCI impairs the neuroregenerative properties of cells used as therapy when obtained from injured animals. We can reasonably hypothesize that this will also be the case in human patients suffering from SCI, in this case calling into question the feasibility and therapeutic effects of such transplants.

Reference

1. Liu Y, Yang X, He Z, Li J, Li Y, Wu Y, et al. Spinal cord injury: global burden from 1990 to 2019 and projections up to 2030 using Bayesian age-period-cohort analysis. Front Neurol. 2023;14:1304153.

2. Golestani A, Shobeiri P, Sadeghi-Naini M, Jazayeri SB, Maroufi SF, Ghodsi Z, et al. Epidemiology of Traumatic Spinal Cord Injury in Developing Countries from 2009 to 2020: A Systematic Review and Meta-Analysis. Neuroepidemiology. 2022;56:219–39.

3. Anjum A, Yazid MD, Fauzi Daud M, Idris J, Ng AMH, Selvi Naicker A, et al. Spinal Cord Injury: Pathophysiology, Multimolecular Interactions, and Underlying Recovery Mechanisms. Int J Mol Sci. 2020;21:7533.

4. Mortazavi MM, Verma K, Harmon OA, Griessenauer CJ, Adeeb N, Theodore N, et al. The microanatomy of spinal cord injury: a review. Clin Anat N Y N. 2015;28:27–36.

5. Anderson MA, Burda JE, Ren Y, Ao Y, O'Shea TM, Kawaguchi R, et al. Astrocyte scar formation aids central nervous system axon regeneration. Nature. 2016;532:195–200.

6. Göritz C, Dias DO, Tomilin N, Barbacid M, Shupliakov O, Frisén J. A pericyte origin of spinal cord scar tissue. Science. 2011;333:238–42.

7. Sabelström H, Stenudd M, Réu P, Dias DO, Elfineh M, Zdunek S, et al. Resident neural stem cells restrict tissue damage and neuronal loss after spinal cord injury in mice. Science. 2013;342:637–40.

8. Anthony DC, Couch Y. The systemic response to CNS injury. Exp Neurol. 2014;258:105–11.

9. Felix M-S, Popa N, Djelloul M, Boucraut J, Gauthier P, Bauer S, et al. Alteration of Forebrain Neurogenesis after Cervical Spinal Cord Injury in the Adult Rat. Front Neurosci. 2012;6.

10. Li Y, Ritzel RM, Khan N, Cao T, He J, Lei Z, et al. Delayed microglial depletion after spinal cord injury reduces chronic inflammation and neurodegeneration in the brain and improves neurological recovery in male mice. Theranostics. 2020;10:11376–403.

11. Benabid AL, Costecalde T, Eliseyev A, Charvet G, Verney A, Karakas S, et al. An exoskeleton controlled by an epidural wireless brain-machine interface in a tetraplegic patient: a proof-of-concept demonstration. Lancet Neurol. 2019;18:1112–22.

12. Lorach H, Galvez A, Spagnolo V, Martel F, Karakas S, Intering N, et al. Walking naturally after spinal cord injury using a brain–spine interface. Nature. 2023;618:126–33.

13. Schneider MP, Sartori AM, Ineichen BV, Moors S, Engmann AK, Hofer A-S, et al. Anti-Nogo-A Antibodies As a Potential Causal Therapy for Lower Urinary Tract Dysfunction after Spinal Cord Injury. J Neurosci Off J Soc Neurosci. 2019;39:4066–76.

14. Boido M, Garbossa D, Fontanella M, Ducati A, Vercelli A. Mesenchymal stem cell transplantation reduces glial cyst and improves functional outcome after spinal cord compression. World Neurosurg. 2014;81:183–90.

15. Yao S, Pang M, Wang Y, Wang X, Lin Y, Lv Y, et al. Mesenchymal stem cell attenuates spinal cord injury by inhibiting mitochondrial quality control-associated neuronal ferroptosis. Redox Biol. 2023;67:102871.

16. Pearse DD, Sanchez AR, Pereira FC, Andrade CM, Puzis R, Pressman Y, et al. Transplantation of Schwann cells and/or olfactory ensheathing glia into the contused spinal cord: Survival, migration, axon association, and functional recovery. Glia. 2007;55:976–1000.

17. Ursavas S, Darici H, Karaoz E. Olfactory ensheathing cells: Unique glial cells promising for treatments of spinal cord injury. J Neurosci Res. 2021;99:1579–97.

18. Assinck P, Duncan GJ, Hilton BJ, Plemel JR, Tetzlaff W. Cell transplantation therapy for spinal cord injury. Nat Neurosci. 2017;20:637–47.

19. Delarue Q, Mayeur A, Chalfouh C, Honoré A, Duclos C, Di Giovanni M, et al. Inhibition of ADAMTS-4 Expression in Olfactory Ensheathing Cells Enhances Recovery after Transplantation within Spinal Cord Injury. J Neurotrauma. 2020;37:507–16.

20. Han D, Wu C, Xiong Q, Zhou L, Tian Y. Anti-inflammatory Mechanism of Bone Marrow Mesenchymal Stem Cell Transplantation in Rat Model of Spinal Cord Injury. Cell Biochem Biophys. 2015;71:1341–7.

21. Gómez RM, Sánchez MY, Portela-Lomba M, Ghotme K, Barreto GE, Sierra J, et al. Cell therapy for spinal cord injury with olfactory ensheathing glia cells (OECs). Glia. 2018;66:1267–301.

22. Solstrand Dahlberg L, Becerra L, Borsook D, Linnman C. Brain changes after spinal cord injury, a quantitative meta-analysis and review. Neurosci Biobehav Rev. 2018;90:272–93.

23. Wu J, Stoica BA, Luo T, Sabirzhanov B, Zhao Z, Guanciale K, et al. Isolated spinal cord contusion in rats induces chronic brain neuroinflammation, neurodegeneration, and cognitive impairment. Involvement of cell cycle activation. Cell Cycle Georget Tex. 2014;13:2446–58.

24. Takano M, Kawabata S, Shibata S, Yasuda A, Nori S, Tsuji O, et al. Enhanced Functional Recovery from Spinal Cord Injury in Aged Mice after Stem Cell Transplantation through HGF Induction. Stem Cell Rep. 2017;8:509–18.

25. Chort A, Alves S, Marinello M, Dufresnois B, Dornbierer J-G, Tesson C, et al. Interferon β induces clearance of mutant ataxin 7 and improves locomotion in SCA7 knock-in mice. Brain J Neurol. 2013;136:1732–45.

26. Robac A, Neveu P, Hugede A, Garrido E, Nicol L, Delarue Q, et al. Repetitive Trans Spinal Magnetic Stimulation Improves Functional Recovery and Tissue Repair in Contusive and Penetrating Spinal Cord Injury Models in Rats. Biomedicines. 2021;9:1827.

27. Ritzel RM, Li Y, He J, Khan N, Doran SJ, Faden AI, et al. Sustained neuronal and microglial alterations are associated with diverse neurobehavioral dysfunction long after experimental brain injury. Neurobiol Dis. 2020;136:104713.

28. Delarue Q, Robac A, Massardier R, Marie J-P, Guérout N. Comparison of the effects of two therapeutic strategies based on olfactory ensheathing cell transplantation and repetitive magnetic stimulation after spinal cord injury in female mice. J Neurosci Res. 2021;99:1835–49.

29. Nakhjavan-Shahraki B, Yousefifard M, Rahimi-Movaghar V, Baikpour M, Nasirinezhad F, Safari S, et al. Transplantation of olfactory ensheathing cells on functional recovery and neuropathic pain after spinal cord injury; systematic review and meta-analysis. Sci Rep. 2018;8:325.

30. M'Dahoma S, Bourgoin S, Hamon M. Neuropathic Pain. Vivo Models Drug Discov. 2014. p. 305–32.

31. Thornton MA, Mehta MD, Morad TT, Ingraham KL, Khankan RR, Griffis KG, et al. Evidence of axon connectivity across a spinal cord transection in rats treated with epidural stimulation and motor training combined with olfactory ensheathing cell transplantation. Exp Neurol. 2018;309:119–33.

32. Khankan RR, Griffis KG, Haggerty-Skeans JR, Zhong H, Roy RR, Edgerton VR, et al. Olfactory Ensheathing Cell Transplantation after a Complete Spinal Cord Transection Mediates Neuroprotective and Immunomodulatory Mechanisms to Facilitate Regeneration. J Neurosci Off J Soc Neurosci. 2016;36:6269–86.

33. Tran AP, Warren PM, Silver J. The Biology of Regeneration Failure and Success After Spinal Cord Injury. Physiol Rev. 2018;98:881–917.

34. Barnabé-Heider F, Göritz C, Sabelström H, Takebayashi H, Pfrieger FW, Meletis K, et al. Origin of new glial cells in intact and injured adult spinal cord. Cell Stem Cell. 2010;7:470–82.

35. Gensel JC, Zhang B. Macrophage activation and its role in repair and pathology after spinal cord injury. Brain Res. 2015;1619:1–11.

36. Anderson MA, O'Shea TM, Burda JE, Ao Y, Barlatey SL, Bernstein AM, et al. Required growth facilitators propel axon regeneration across complete spinal cord injury. Nature. 2018;561:396–400.

37. Irvine SF, Kwok JCF. Perineuronal Nets in Spinal Motoneurones: Chondroitin Sulphate Proteoglycan around Alpha Motoneurones. Int J Mol Sci. 2018;19:1172.

38. Grycz K, Głowacka A, Ji B, Krzywdzińska K, Charzyńska A, Czarkowska-Bauch J, et al. Regulation of perineuronal net components in the synaptic bouton vicinity on lumbar α-motoneurons in the rat after spinalization and locomotor training: New insights from spatio-temporal changes in gene, protein expression and WFA labeling. Exp Neurol. 2022;354:114098.

39. Noble BT, Brennan FH, Popovich PG. The spleen as a neuroimmune interface after spinal cord injury. J Neuroimmunol. 2018;321:1–11.

40. Gris D, Hamilton EF, Weaver LC. The systemic inflammatory response after spinal cord injury damages lungs and kidneys. Exp Neurol. 2008;211:259–70.

41. Anthony DC, Couch Y. The systemic response to CNS injury. Exp Neurol. 2014;258:105–11.

42. Farkas GJ, Gorgey AS, Dolbow DR, Berg AS, Gater DR. The influence of level of spinal cord injury on adipose tissue and its relationship to inflammatory adipokines and cardiometabolic profiles. J Spinal Cord Med. 2018;41:407–15.

43. Felix M-S, Popa N, Djelloul M, Boucraut J, Gauthier P, Bauer S, et al. Alteration of forebrain neurogenesis after cervical spinal cord injury in the adult rat. Front Neurosci. 2012;6:45.

44. Capirossi R, Piunti B, Fernández M, Maietti E, Rucci P, Negrini S, et al. Early CSF Biomarkers and Late Functional Outcomes in Spinal Cord Injury. A Pilot Study. Int J Mol Sci. 2020;21:9037.

45. Delarue Q, Guérout N. Transplantation of Olfactory Ensheathing Cells: Properties and Therapeutic Effects after Transplantation into the Lesioned Nervous System. Neuroglia. 2022;3:1–22.

46. Gueye Y, Ferhat L, Sbai O, Bianco J, Ould-Yahoui A, Bernard A, et al. Trafficking and secretion of matrix metalloproteinase-2 in olfactory ensheathing glial cells: A role in cell migration? Glia. 2011;59:750–70.

47. Honoré A, Le Corre S, Derambure C, Normand R, Duclos C, Boyer O, et al. Isolation, characterization, and genetic profiling of subpopulations of olfactory ensheathing cells from the olfactory bulb. Glia. 2012;60:404–13.

48. Zhang L, Zhuang X, Kotitalo P, Keller T, Krzyczmonik A, Haaparanta-Solin M, et al. Intravenous transplantation of olfactory ensheathing cells reduces neuroinflammation after spinal cord injury via interleukin-1 receptor antagonist. Theranostics. 2021;11:1147–61.

49. Radtke C, Akiyama Y, Brokaw J, Lankford KL, Wewetzer K, Fodor WL, et al. Remyelination of the nonhuman primate spinal cord by transplantation of H-transferase transgenic adult pig olfactory ensheathing cells. FASEB J Off Publ Fed Am Soc Exp Biol. 2004;18:335–7.

50. Macias MY, Syring MB, Pizzi MA, Crowe MJ, Alexanian AR, Kurpad SN. Pain with no gain: allodynia following neural stem cell transplantation in spinal cord injury. Exp Neurol. 2006;201:335–48.

51. Tansley S, Gu N, Guzmán AU, Cai W, Wong C, Lister KC, et al. Microglia-mediated degradation of perineuronal nets promotes pain. Science. 2022;377:80–6.

52. Zhou X, He X, Ren Y. Function of microglia and macrophages in secondary damage after spinal cord injury. Neural Regen Res. 2014;9:1787–95.

53. Bellver-Landete V, Bretheau F, Mailhot B, Vallières N, Lessard M, Janelle M-E, et al. Microglia are an essential component of the neuroprotective scar that forms after spinal cord injury. Nat Commun. 2019;10:518.

54. Brennan FH, Li Y, Wang C, Ma A, Guo Q, Li Y, et al. Microglia coordinate cellular interactions during spinal cord repair in mice. Nat Commun. 2022;13:4096.

Figure legends:

Figure 1: Schematic representation of the four main experimental groups used in our study.

A. No SCI group, uninjured animals used to define the baselines for functional and histological experiments. **B**. SCI group, injured animals without treatment. **C**. SCI bOECs H, SCI was performed on these animals and primary bOEC transplantation was performed immediately after SCI. OB used to prepare bOEC cultures was obtained from uninjured animals. **D**. SCI bOECs I, SCI was performed on these animals and primary bOEC transplantation was performed immediately after SCI. OB used to prepare primary bOEC cultures were obtained from previously SCI injured animals. This SCI was performed on a different set of mice 7 days prior to the primary OB cultures.

Figure 2: SCI alters cellular reactivity in olfactory bulbs and gene expression in cells in primary bOEC cultures.

A. Representative images of sagittal section of the OB, representative of the granular cell layer. Sections were stained with anti-Iba1 and anti-CD86 antibodies. Microglial cell reactivity was analyzed by expression of Iba1 and CD86 markers. Arrows show Iba1+/CD86+ microglial cells. Scale bare: A1=250 µm, A2=100 µm and A3=20 µm. **B-D**. Chronology of microglial cell reactivity in the OB. The expression of the cells markers Iba1 (**B**) and CD86 (**C**) and the percentage of Iba1+/CD86+ cells (**D**) were measured without SCI and 3, 6, 12, 24, 48 hours and 7 days after SCI. **E**. Experimental design for bOEC H and bOEC I cultures characterization after SCI. Mice received SCI on day 0. Seven days after SCI, OB were collected from uninjured and 7d injured mice to establish, bOEC H (No SCI) and 7d bOEC I (SCI 7d) primary cultures, respectively. Fourteen days after SCI, OB were collected from 14d injured mice to realized 14d bOEC I (SCI 14d) primary culture. At day 35, No SCI and SCI 7d primary cultures were characterized by cytometry and RT-qPCR. Characterization of SCI 14d primary culture was performed on day 42. **F**. Quantification of the percentage of p75+ OECs and PDGFRβ+ fibroblasts in bOEC cultures without SCI, 7 days and 14 days after SCI by cytometric analyses. **G**. Histograms of bOECs H and bOECs I mRNA expression of immunomodulatory, axonal plasticity, ECM/signaling and growth factor genes. Dashed lines correspond to mRNA expression from bOEC H cultures used as control. Quantifications are expressed as average ± SD. N=5 (**B-D**), 3 (**F**) and 8 (**G**) animals per group. Statistical evaluations were based on Mann-Whitney (**F** and **G**) and Kruskal-Wallis (**B-D**) tests. * = $P < 0.05$, ** = $P < 0.01$ and *** = $P < 0.001$.

Figure 3: The survival of bOECs from injured mice is identical to that of bOECs from healthy mice after transplantation.

A. Representative images of LUX+/- bOEC H and LUX +/- bOEC I cultures transplanted into wild type mice 7 and 21 days after SCI and transplantation. **B**. Quantification of luciferase+ signals 7, 14 and 21 days after SCI. **C**. Quantification of mean fluorescence intensity of the bOECs tdTomato H and I, 14, 21 and 28 days after SCI. **D**. Representative images of sagittal spinal cord sections from SCI bOECs H tdTomato and SCI bOECs I tdTomato groups 14, 21 and 28 days after SCI. Dashed lines correspond to the injury site. Scale bar = 250 µm. Quantifications are expressed as average ± SD. N=3 (**B**) and 5 (**C**) animals per group. Statistical evaluations were based on Kruskal-Wallis tests.

Figure 4: Transplantation of bOECs from injured mice resulted in less functional recovery than bOECs from healthy mice.

A. Experimental design for experiments on motor behavior. Mice received SCI and bOEC H or I transplantation on day 0. Fourteen, twenty-eight and fifty-six days after SCI, functional analyses were performed. **B**. Schematic representation of the Locotronic test. **C**-**K**. Functional recovery was analyzed using Locotronic test 14, 28 and 56 days after SCI. Dashed lines correspond to the baseline parameters obtained during Locotronic test habituation (7 days before SCI). **C**, **F** and **I**. Quantification of the number of hindlimb errors. **D**, **G** and **J**. Quantification of the total hindlimb errors time. **E**, **H** and **K**. Quantification of the total crossing time. **L**. Schematic representation of the CatWalk test. **M** and **N**. CatWalk gait analysis was performed 56 days after SCI. Green and red dashed lines corresponds respectively to the baseline parameters obtained with CatWalk gait analysis during habituation (7 days before SCI) and to the parameters obtained by SCI group 56 days after SCI. **M**. Measurement of the base of support (BOS). **N**. Measurement of the stride length. **O**. Example of photographs taken during the CatWalk gait for analyses. 1- SCI group, 2- SCI + bOECs H group, 3- SCI + bOECs I group. Quantifications are expressed as average $\pm$ SD. N=8-10 (**C**-**H**), 5-10 **(I**-**K**) and 5 (**M** and **N**) animals per group. Statistical evaluations were based on Kruskal-Wallis (**C**-**K**) and Mann-Whitney (**M** and **N**) tests. Quantifications are expressed as average $\pm$ SD. * = $P < 0.05$; ** = $P < 0.01$ and *** = $P < 0.001$.

Figure 5: The tissue repair properties induced by transplanting bOECs from healthy mice are not achieved by transplanting bOECs from injured mice.

Histological analyses of the spinal scar were performed 14, 28 and 56 days after SCI. **A, E** and **I**. Representative pictures of sagittal spinal cord sections of SCI, SCI bOECs H and SCI bOECs I groups 14 (**A**), 28 (**E**) and 56 (**I**) days after SCI. Sections were stained with anti-GFAP, anti-PDGFRβ and anti-MBP antibodies. **B, F** and **J**. Quantification of fibrosis areas (PDGFRβ+) 14 (**B)**, 28 (**F**) and 56 (**J**) days after SCI. **C, G** and **K**. Quantification of astrocyte-free areas (GFAP-) 14 (**C**), 28 (**G**) and 56 (**K**) days after SCI. **D, H** and **L**. Quantification of demyelinated/unmyelinated area (MBP-) 14 (**D**), 28 (**H**) and 56 (**L**) days after SCI. **M**-**O**. Representation of changes over time of the three analyses: PDGFRβ+ (**M**), GFAP- (**N**) and MBP- (**O**). **A, E** and **I**. Dashed lines correspond to the injury site. Scale bar = 200 µm.

Quantifications are expressed as average ± Min/Max. N=8-10 (**B, C, D, F, G** and **H**), 5-10 (**J-L**) animals per group. Statistical evaluations were based on Kruskal-Wallis tests. Quantifications are expressed as average ± SD. * = $P < 0.05$ and ** = $P < 0.01$.

Figure 6: Transplantation of bOECs induces axonal regrowth, but this regrowth is associated with synaptogenesis and pain-related behavior only in mice that received bOECs from healthy mice.

A. Experimental design for experiments on sensory behavior. Mice received SCI and bOEC H or I transplantation on day 0. Fourteen, twenty-eight and fifty-six days after SCI, functional analyses and immunohistology were performed. (**B**) Functional sensory recovery was analyzed 14, 28 and 56 days after SCI, using the Hargreaves test. Dashed lines correspond to the baseline results obtained during the Hargreaves test habituation (7 days before SCI). **C** and **D**. CatWalk gait analysis was performed. Quantification of hindpaw pressure measurements, maximum (**C**) and mean (**D**) hindpaw pressure measurements at 56 days after SCI. Green and red dashed lines correspond respectively to the baseline results obtained during the CatWalk gait test habituation (7 days before SCI) and to the results obtained by the SCI group 56 days after SCI. In addition, (**E-L**) histological analyses were performed 14, 28 and 56 days after SCI. **E-F**. Laminin expression was analyzed as a support for axonal growth. Quantification of laminin+ area/ PDGFRβ+ area ratio (**E**) 14, 28 and 56 days after SCI. **F**. Representative images of sagittal spinal cord sections from SCI bOECs I group 14 days after SCI, showing the laminin area and corresponding PDGFRβ area. Sections were stained with anti-laminin antibody and anti- PDGFRβ antibodies. Scale bar = 500 µm. **G-H**. Representative images of sagittal spinal cord sections from SCI bOECs I group. **G**. The square sections correspond to the rostral (R), lesion core (LC) and caudal (C) areas, defined for quantification of BDA+/vGlut1+ axon sprouting. The rectangular sections correspond to the areas defined for the quantification of axon sprouting as a function of distance from the lesion core. Arrows indicate axon sprouting (**G**) and co-localized BDA+/vGlut1+ axon (**H**). Sections were stained with (**G**) biotinylated BDA and anti-PDGFRβ antibody and (**H**) biotinylated BDA and anti-vGlut1 antibody. Scale bar = 500 µm (**G**) and 100 µm (**H**). **I-K**.

The number of sprouting axons as a function of distance from the lesion core was counted 14, 28 and 56 days after SCI. **L**. Sprouting axons co-localized with synaptic vGlut1+ were counted 14, 28 and 56 days after SCI.

Quantifications are expressed as average ± SD (**B, C, D, I, J, K,** and **L**) and average ± Min/Max (**E**). N=6-10 (**B** and **E**) and 5 (**C, D, I, J, K,** and **L**) animals per group. Statistical evaluations were based on Kruskal-Wallis (**B, E, I, J, K,** and **L**) and Mann-Whitney (**C** and **D**) tests. * = $P < 0.05$; ** = $P < 0.01$ and *** = $P < 0.001$.

Figure 7: Transplantation of bOECs from healthy and injured mice affects neuronal survival and perineural network structure differently.

Histological analyses of the neuronal density and stability. **A**-**C**. Representative images of sagittal spinal cord sections from SCI (**A**), SCI bOECs H (**B**) and SCI bOECs I (**C**) groups 14 days after SCI. Section were stained with anti-NeuN antibody and biotinylated WFA. The square sections correspond to the rostral 1 and 2 (R1 and R2), lesion core (LC) and caudal 1 and 2 (C1 and C2) areas, defined for the quantification of NeuN+ neurons and WFA+ perineural net. Arrows indicate co-localized NeuN and WFA staining. Scale bar = 250 µm (sagittal spinal cord sections) and 100 µm (R2, R1, LC, C1 and C2 squares analyzed). **D**, **G** and **J**. Quantification of the neuronal density 14 (**D**), 28 (**G**) and 56 (**J**) days after SCI. **E**, **F**, **H**, **I**, **K** and **L**. Analysis of the perineural net. **E**, **H** and **K**. Quantification of the number of NeuN+ neurons surrounded by WFA 14 (**E**), 28 (**H**) and 56 (**K**) days after SCI. **F**, **I** and **L**. Measurement of WFA intensity 14 (**F**), 28 (**I**) and 56 (**L**) days after SCI. Dashed lines correspond to the baseline parameters obtained in the No SCI group. Quantifications are expressed as average $\pm$ SD. N=5-8 (**D**-**F**), 5-10 (**G**-**I**) and 5 (**J**-**L**) animals per group. Statistical analysis was based on Kruskal-Wallis test. * = $P < 0.05$ and ** = $P < 0.01$.

Figure 8: Transplantation of bOECs from healthy and injured mice alters microglia/macrophages polarization.

A-I. Histological analysis of microglia/macrophage cell density and polarization. **A.** The number of Iba1 positive microglia/macrophage cells was measured 14, 28 and 56 days after SCI. **B** and **C**. Representative images of sagittal spinal cord sections from SCI, SCI bOECs H and SCI bOECs I groups 28 days after SCI. Sections were stained with anti-Iba1 and anti-CD86 antibodies (**B**) and anti-Iba1 and anti-CD206 antibodies (**C**). The square sections correspond to the rostral (R), lesion core (LC) and caudal (C) areas, defined for the quantification of Iba1+/CD86+ and Iba1+/CD206+ cells. Arrows indicate Iba1+/CD86+ microglial cells (**B**) and Iba1+/CD206+ microglial cells (**C**). Scale bar = 250 µm (sagittal spinal cord sections) and 100 µm (Squares analysed in R, LC and C). Microglia/macrophage polarization was analyzed by expression of pro-inflammatory marker CD86 (**D, F** and **H**) and anti-inflammatory marker CD206 (**E, G** and **I**) at 14 (**D** and **E**), 28 (**F** and **G**) and 56 (**H** and **I**) days post SCI. **J-M**. Induction of BV2 cells polarization *in vitro* by bOECs conditioned medium (CM). **J**. Experimental design, healthy or injured bOECs were plated (day 0). Four weeks after plating, bOECs H and bOECs I CM were collected and concentrated (day 28). BV2 cells were plated (day 29) and the next day (day 30), bOECs H or bOECs I concentrated CM was added to the BV2 cell cultures. Two days after (day 32), BV2 cells were removed from the plates and analyzed by RT-qPCR. **K-M**. Histogram of mRNA expression of BV2 cell control and BV2 cells with bOECs H CM or bOECs I CM of cytokine, chemokine, trophic factor and receptor genes. Dashed lines correspond to mRNA expression from control BV2 cells cultures. Quantifications are expressed as average ± SD (**D**, **E**, **F**, **G**, **H**, **I**, **K**, **L** and **M**) and average ± Min/Max (**A**). N=5-10 (**A**), 8-10 (**D-G**) and 5-10 (**H** and **I**) animals per group. N=5 BV2 cell cultures (**K, L** and **M**) per group. Statistical analyses were

based on Kruskal-Wallis (**A, D, E, F, G, H** and **I**) and Mann-Whitney (**K, L** and **M**) tests. * and γ = P< 0.05; ** = P< 0.01 and *** = P< 0.001.

Table 1: Table of genes for immunity and inflammatory molecules analyzed by qRT-PCR. This table lists the gene abbreviation, full name, function and NCBI gene ID of 49 immune and inflammatory molecules for which gene expression levels were analyzed in this study.

Table 2: Table of genes for axonal growth inhibitory and axonal growth permissive molecules analyzed by qRT-PCR. This table lists the gene abbreviation, full name, function and NCBI gene ID of 84 axon growth modulating molecules for which gene expression levels were analyzed in this study [5].

Table 1:

Gene abbreviation	Molecule name	Fonction	NCBI gene ID
Actb	Actin, beta	Housekeeping gene	11461
Arg1	Arginase 1	Metabolic enzyme	11846
B2m	Beta- 2 microglobulin	Housekeeping gene	12010
Bdnf	Brain derived neurotrophic factor	Growth Factor	12064
Ccl5	Chemokine (C-C motif) ligand 5	Chemokine	20304
Ccr2	Chemokine (C-C motif) receptor 2	Receptor	12772
Ccr5	Chemokine (C-C motif) receptor 5	Receptor	12774
Csf1	Colony stimulating factor 1 (macrophage)	Growth Factor	12977
Cx3cl1	Chemokine (C-X3-C motif) ligand 1	Chemokine	20312
Cx3cr1	Chemokine (C-X3-C) receptor 1	Chemokine	13051
Cxcl12	Chemokine (C-X-C motif) ligand 12	Chemokine	20315
Cxcr3	Chemokine (C-X-C motif) receptor 3	Receptor	12766
Cxcr4	Chemokine (C-X-C motif) receptor 4	Receptor	12767
Fas	Fas (TNF receptor superfamily member 6)	Receptor	14102
Gapdh	Glyceraldehyde-3-phosphate dehydrogenase	Housekeeping gene	14433
Gdnf	Glial cell line derived neurotrophic factor	Growth Factor	14573
Ifng	Interferon gamma	Cytokine	15978
Ifngr1	Interferon gamma receptor 1	Receptor	15979
Ifngr2	Interferon gamma receptor 2	Receptor	15980
Igf1	Insulin- like growth factor 1	Growth Factor	16000
Il10ra	Interleukin 10 receptor, alpha	Receptor	16154
Il10rb	Interleukin 10 receptor, beta	Receptor	16155
Il18	Interleukin 18	Cytokine	16173
Il1a	Interleukin 1 alpha	Cytokine	16175
Il1b	Interleukin 1 beta	Cytokine	16176
Il6ra	Interleukin 6 receptor, alpha	Receptor	16194
Irf1	Interferon regulatory factor 1	Transcriptional Regulator	16362
Irf3	Interferon regulatory factor 3	Transcriptional Regulator	54131
Irf9	Interferon regulatory factor 9	Transcriptional Regulator	16391
Mrc1	Mannose receptor, C type 1	Receptor	17533
Myd88	Myeloid differentiation primary response	Transcriptional Regulator	17874
Nfkb1	Nuclear factor of kappa light polypeptide gene enhancer in B-cells 1	Transcriptional Regulator	18033
Nos2	Nitric oxide synthase 2, inducible	Metabolic enzyme	18126
P2rx4	Purinergic receptor P2X, ligand-gated ion channel 4	Receptor	18438
P2rx7	Purinergic receptor P2X, ligand-gated ion channel 7	Receptor	18439
P2ry12	Purinergic receptor P2Y, G-protein coupled 12	Receptor	70839
P2ry6	Purinergic receptor P2Y, G-protein coupled 6	Receptor	233571
Sod1	Superoxide dismutase 1, soluble	Transcriptional Regulator	20655
Tgfb1	Transforming growth factor, beta 1	Cytokine	21803
Tgfb2	Transforming growth factor, beta 2	Cytokine	21808
Tgfbr1	Transforming growth factor, beta receptor I	Receptor	21812
Tlr4	Toll- like receptor 4	Receptor	21898
Tlr9	Toll- like receptor 9	Receptor	81897
Tnf	Tumor necrosis factor	Cytokine	21926
Tnfrsf1a	Tumor necrosis factor receptor superfamily, member 1a	Receptor	21937
Tnfrsf1b	Tumor necrosis factor receptor superfamily, member 1b	Receptor	21938
Trem2	Triggering receptor expressed on myeloid cells 2	Receptor	83433
Vegfa	Vascular endothelial growth factor A	Growth Factor	22339
Vegfb	Vascular endothelial growth factor B	Growth Factor	22340

Table 2:

Gene abbreviation	Molecule name	Fonction	NCBI gene ID
Acan	Aggrecan	ECM & Adhesion	11595
Actb	Actin beta	Housekeeping genes	11461
Adam10	ADAM metallopeptidase domain 10	ECM & Adhesion	11487
Bcan	Brevican	ECM & Adhesion	12032
Bdnf	Brain derived neurotrophic factor	Growth Factor	12064
B2m	Beta-2-microglobulin	Housekeeping gene	12010
Ccl2	C-C Motif Chemokine Ligand 2	Immunomodulatory	20296
Cntf	Ciliary Neurotrophic Factor	Axonal and synaptic plasticity	12803
Col1a1	Collagen type I alpha 1 chain	ECM & Adhesion	12842
Col3a1	Collagen type III alpha 1 chain	ECM & Adhesion	12825
Col4a1	Collagen type IV alpha 1 chain	ECM & Adhesion	12826
Cspg4	Chondroitin sulfate proteoglycan NG2	ECM & Adhesion	121021
Cspg5	Neuroglycan C	ECM & Adhesion	29873
Ctgf	Connective tissue growth factor	Growth Factor	14219
Dcc	DCC netrin 1 receptor	Axonal and synaptic plasticity	13176
Dcn	Decorin	ECM & Adhesion	13179
Efnb3	Ephrin B3	Axonal and synaptic plasticity	13643
Eg-vegf	Prokineticin 1	Growth Factor	246691
Epha4	EPH receptor A4	Axonal and synaptic plasticity	13838
Ephb2	EPH receptor B2	ECM & Adhesion	13844
Flt1	Fms related tyrosine kinase 1	Growth Factor	14254
Flt4	Fms related tyrosine kinase 4	Growth Factor	14257
Fn1	Fibro,ectin 1	ECM & Adhesion	14268
Fgf1	Fibroblast growth factor 1	Growth Factor	14164
Fgf2	Fibroblast growth factor 2	Growth Factor	14173
Gapdh	Glyceraldehyde-3-phosphate dehydrogenase	Housekeeping gene	14433
Gdnf	Glial derived neurotrophic factor	Growth Factor	14573
Gpc1	Glypican 1	ECM & Adhesion	14733
Gpc3	Glypican 3	ECM & Adhesion	14734
Gpc5	Glypican 5	ECM & Adhesion	103978
Gusb	Glucoronidase beta	Housekeeping gene	110006
Hsp90ab1	Heat shock protein 90 alpha class B member 1	Housekeeping gene	15516
Ifng	Interferon gamma	Immunomodulatory	15978
Igf1	Insulin like growth factor 1	Growth Factor	16000
Il1b	Interleukine 1 beta	Immunomodulatory	16176
Il6	Interleukine 6	Immunomodulatory	16193
Kdr	Kinase insert domain receptor	Growth Factor	16542
Lamc1	Laminin C 1	ECM & Adhesion	226519
Lglas1	Galectin 1	ECM & Adhesion	16852
Matn2	Matrilin 2	ECM & Adhesion	17181
Mcam	Melanoma cell adhesion molecule	ECM & Adhesion	84004
Mmp2	Matrix metallopeptidase 2	ECM & Adhesion	17390
Mmp9	Matrix metallopeptidase 9	ECM & Adhesion	17395
Met	MET proto-oncogene, receptor tyrosine kinase	Growth Factor	17295
Ncam1	Neural cell adhesion molecule 1	ECM & Adhesion	17967
Ncan	Neurocan	ECM & Adhesion	13004
Neo1	Neogenin 1	ECM & Adhesion	18007
Ntf3	Neurotrophin 3	Growth Factor	18205
Nrp1	Neuropilin 1	Axonal and synaptic plasticity	18186
Ntn1	Netrin 1	Axonal and synaptic plasticity	18208
Pdgfa	Platelet derived growth factor subunit a	Growth Factor	18590
Pgf	Pacental growth factor	Growth Factor	18654
Plxna1	Plexin A1	Axonal and synaptic plasticity	18844
Plxnb1	Plexin B1	Axonal and synaptic plasticity	235611
Rgma	Repulsive guidance molecule BMP co-receptor A	Axonal and synaptic plasticity	244058
Rgmb	Repulsive guidance molecule BMP co-receptor B	Axonal and synaptic plasticity	68799
Robo1	Roundaout guidance receptor 1	Axonal and synaptic plasticity	19876
Robo2	Roundaout guidance receptor 2	Axonal and synaptic plasticity	268902
Sdc1	Syndecan 1	ECM & Adhesion	20969
Sdc2	Syndecan 2	ECM & Adhesion	15529
Sdc3	Syndecan 3	ECM & Adhesion	20970
Sdc4	Syndecan 4	ECM & Adhesion	20971
Sema3a	Semaphorin 3A	Axonal and synaptic plasticity	20346
Sema3f	Semaphorin 3F	Axonal and synaptic plasticity	20350
Serpinf1	Serpin family F member 1	ECM & Adhesion	20317
Slit 1	Slit guidance ligand 1	Axonal and synaptic plasticity	20562
Slitrk1	SLIT and NTRK like family member 1	Axonal and synaptic plasticity	76965
Tek	TEK receptor tyrosine kinase	Growth Factor	21687
Tgfa	Transforming growth factor alpha	Growth Factor	21802
Tgfb1	Transforming growth factor beta 1	Growth Factor	21803
Tgfb2	Transforming growth factor beta 2	Growth Factor	21808
Tgfb3	Transforming growth factor beta 3	Growth Factor	21809
Thbs1	Thrombospondin 1	ECM & Adhesion	21825
Thbs2	Thrombospondin 2	ECM & Adhesion	21826
Timp1	Tissue Inhibitor Of Metalloproteinases 1	ECM & Adhesion	21857
Timp2	Tissue Inhibitor Of Metalloproteinases 2	ECM & Adhesion	21858
Tnc	Tenascin C	Axonal and synaptic plasticity	21923
Tnf	Tumoral necrosis factor	Immunomodulatory	21926
Tnr	Tenascin R	Axonal and synaptic plasticity	21960
Vcan	Versican	ECM & Adhesion	13003
Vegfa	Vascular endothelial growth factor A	Growth Factor	22339
Vegfb	Vascular endothelial growth factor B	Growth Factor	22340
Ve-cad	Vascular endothelial cadherin	ECM & Adhesion	12562
Xylt1	Xylosyltransferase 1	ECM & Adhesion	233781

Fig 1:

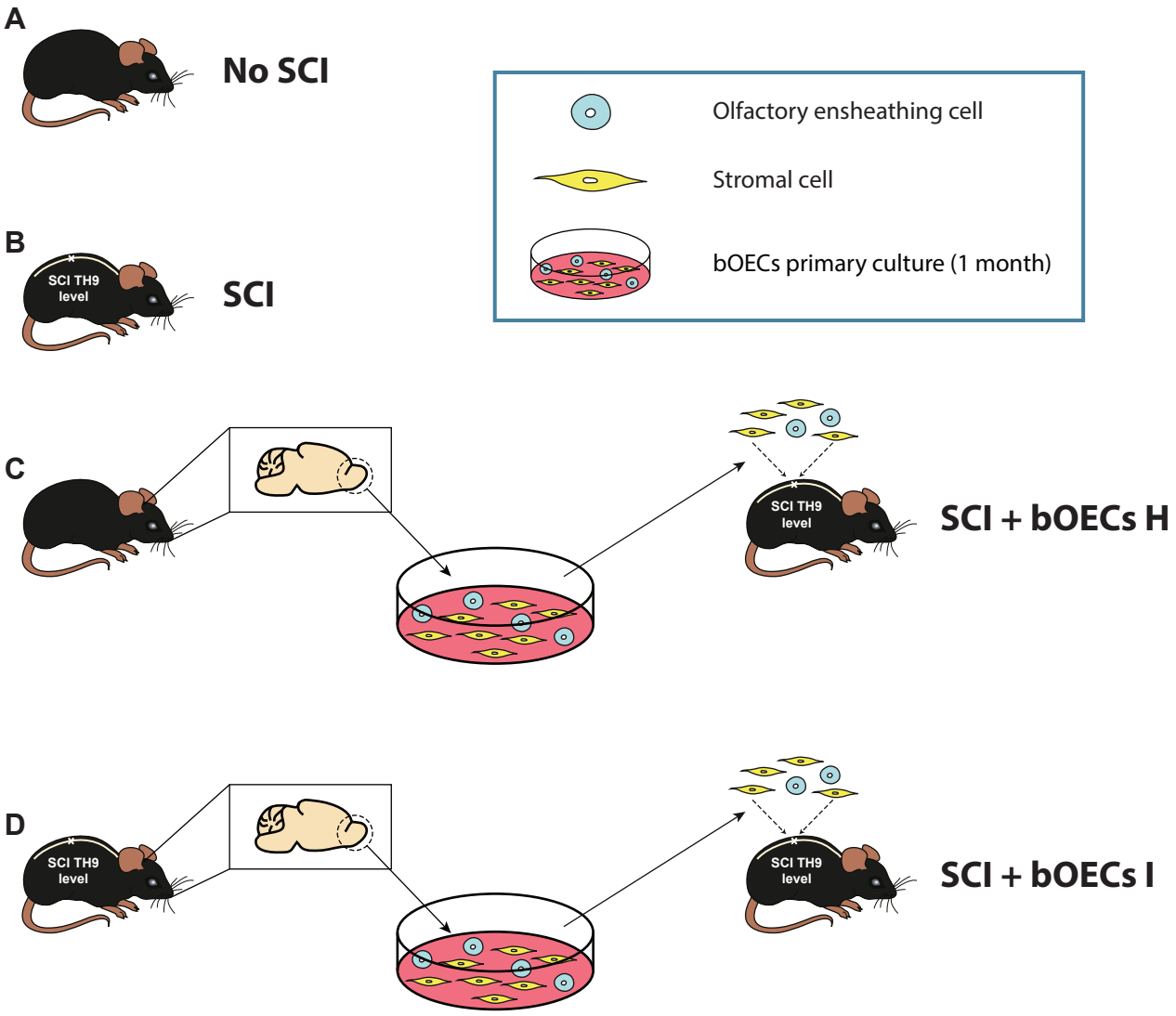
A
No SCI
Olfactory ensheathing cell
Stromal cell
bOECs primary culture (1 month)
B
SCI TH9 level
SCI
C
SCI TH9 level
SCI + bOECs H
D
SCI TH9 level
SCI TH9 level
SCI + bOECs I

Fig 2:

In vivo

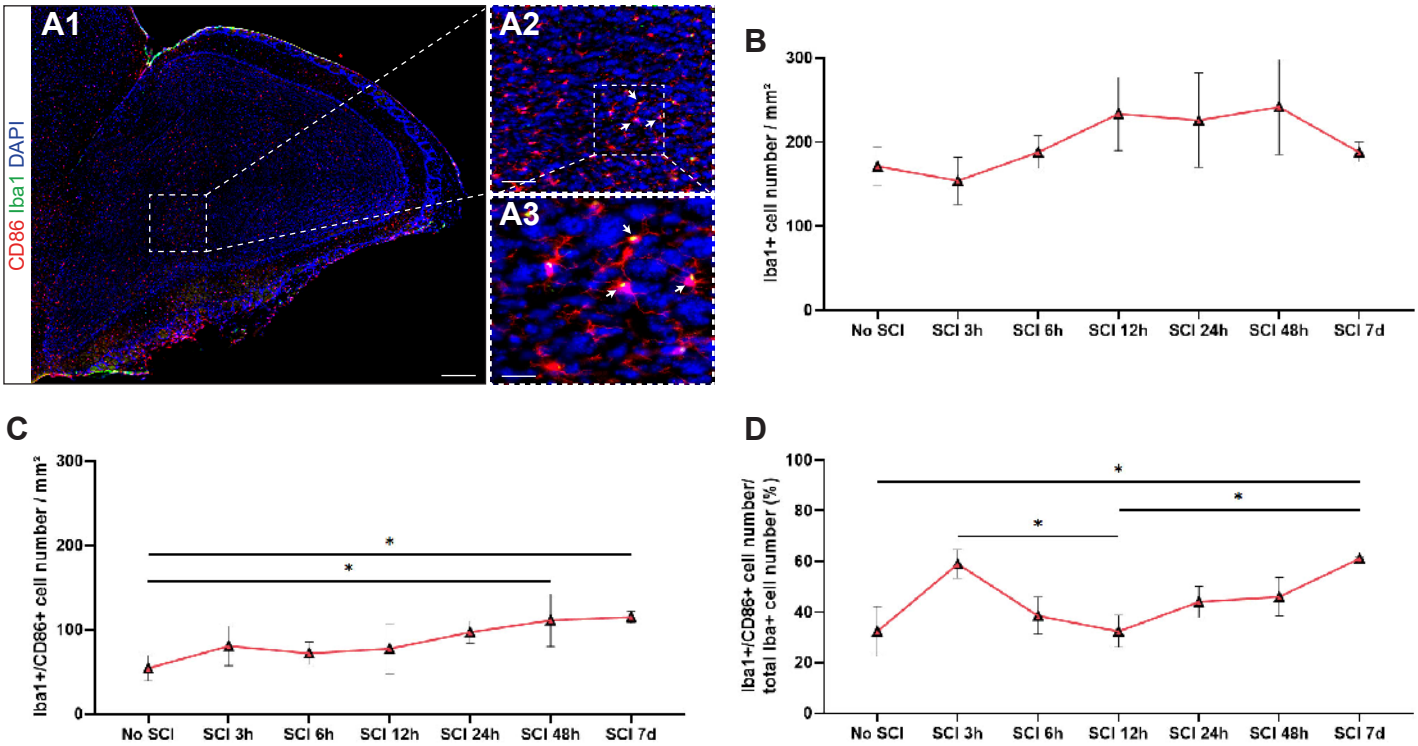

In vitro

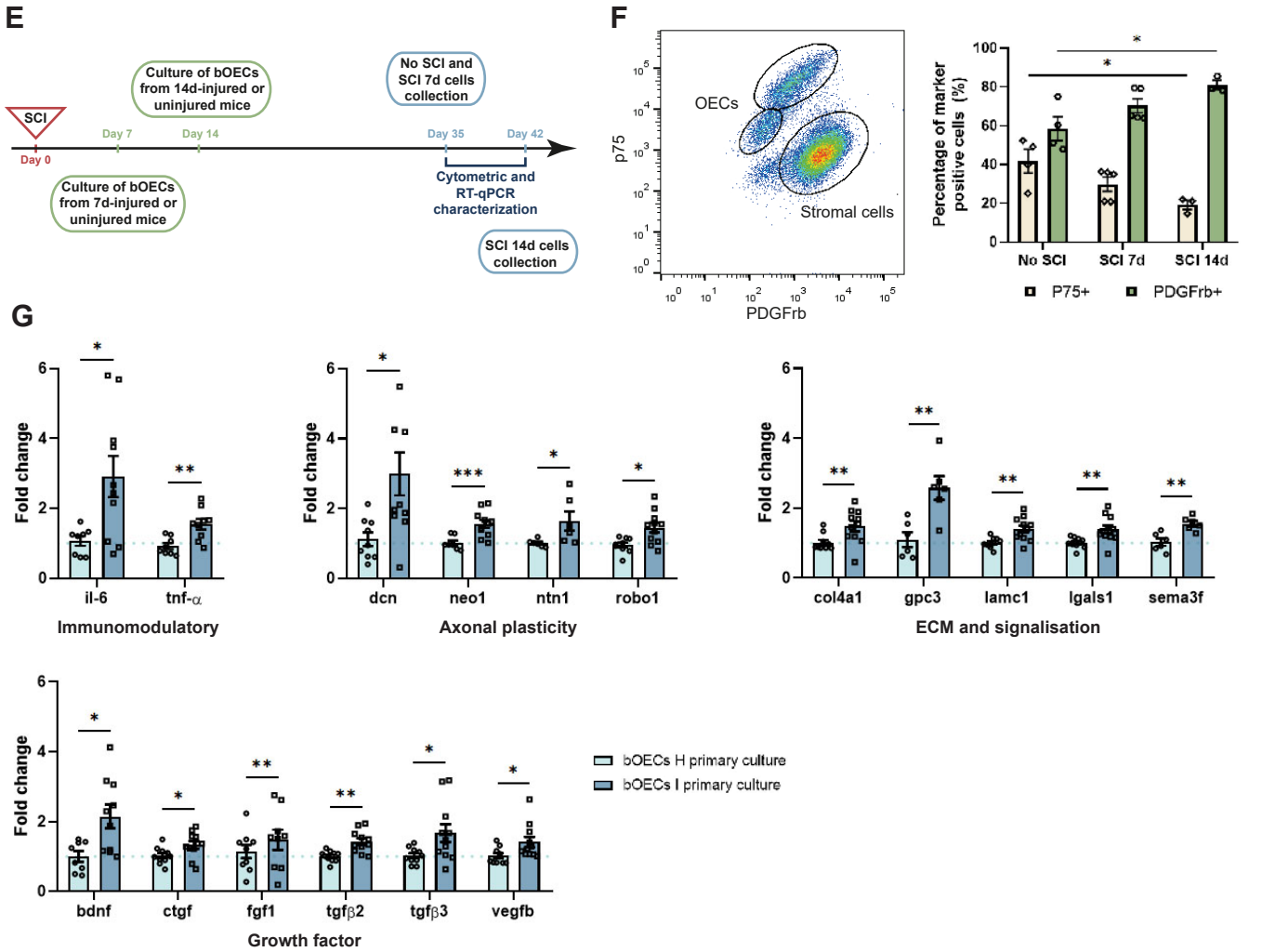

Fig 3:

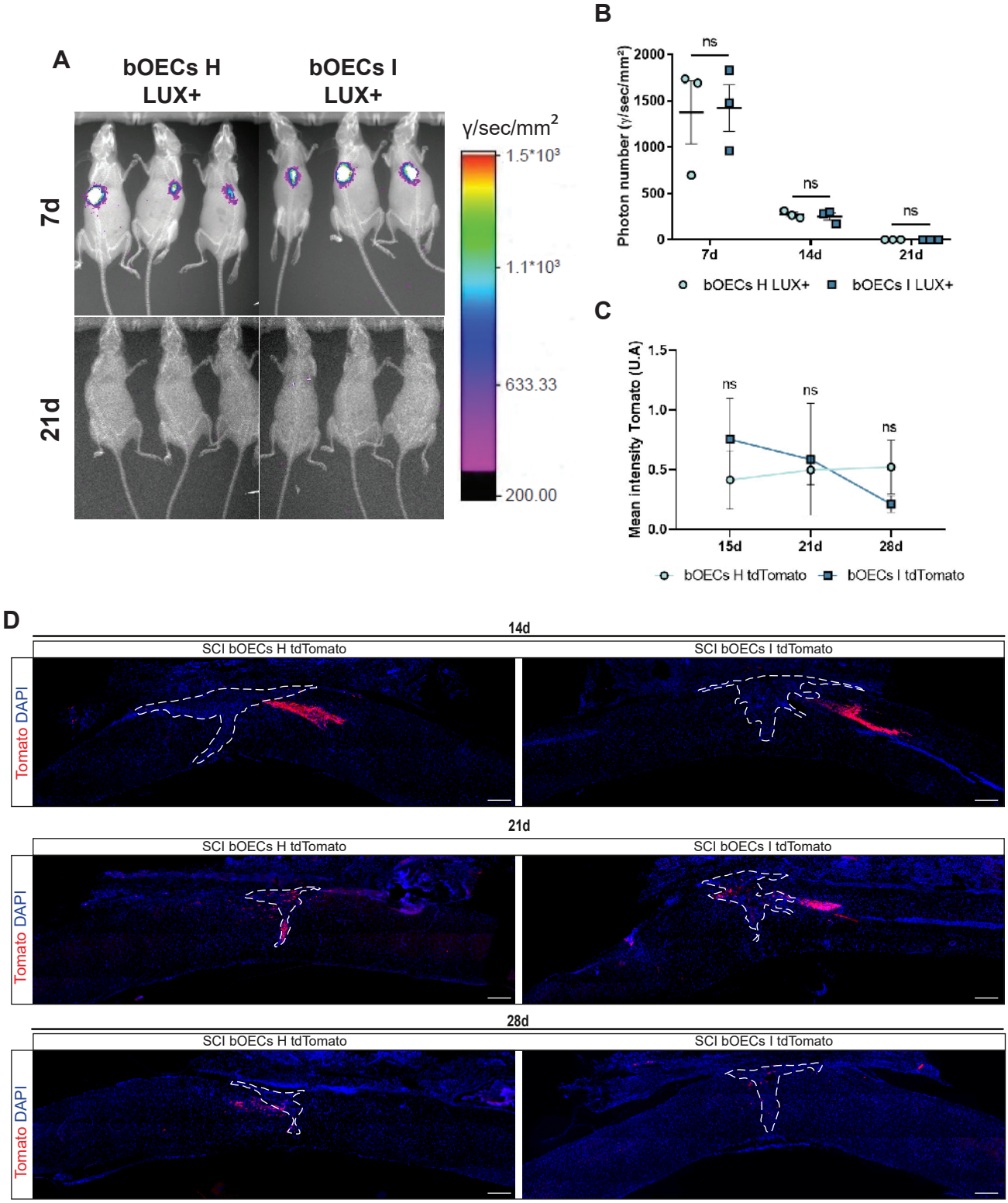
A
bOECs H LUX+
bOECs I LUX+
7d
21d
γ/sec/mm²
1.5*10³
1.1*10³
633.33
200.00
B
Photon number (γ/sec/mm²)
2000
1500
1000
500
0
ns
ns
ns
7d
14d
21d
bOECs H LUX+
bOECs I LUX+
C
Mean intensity Tomato (U.A)
1.5
1.0
0.5
0.0
ns
ns
ns
15d
21d
28d
bOECs H tdTomato
bOECs I tdTomato
D
14d
SCI bOECs H tdTomato
SCI bOECs I tdTomato
Tomato DAPI
21d
SCI bOECs H tdTomato
SCI bOECs I tdTomato
Tomato DAPI
28d
SCI bOECs H tdTomato
SCI bOECs I tdTomato
Tomato DAPI

Fig 4:

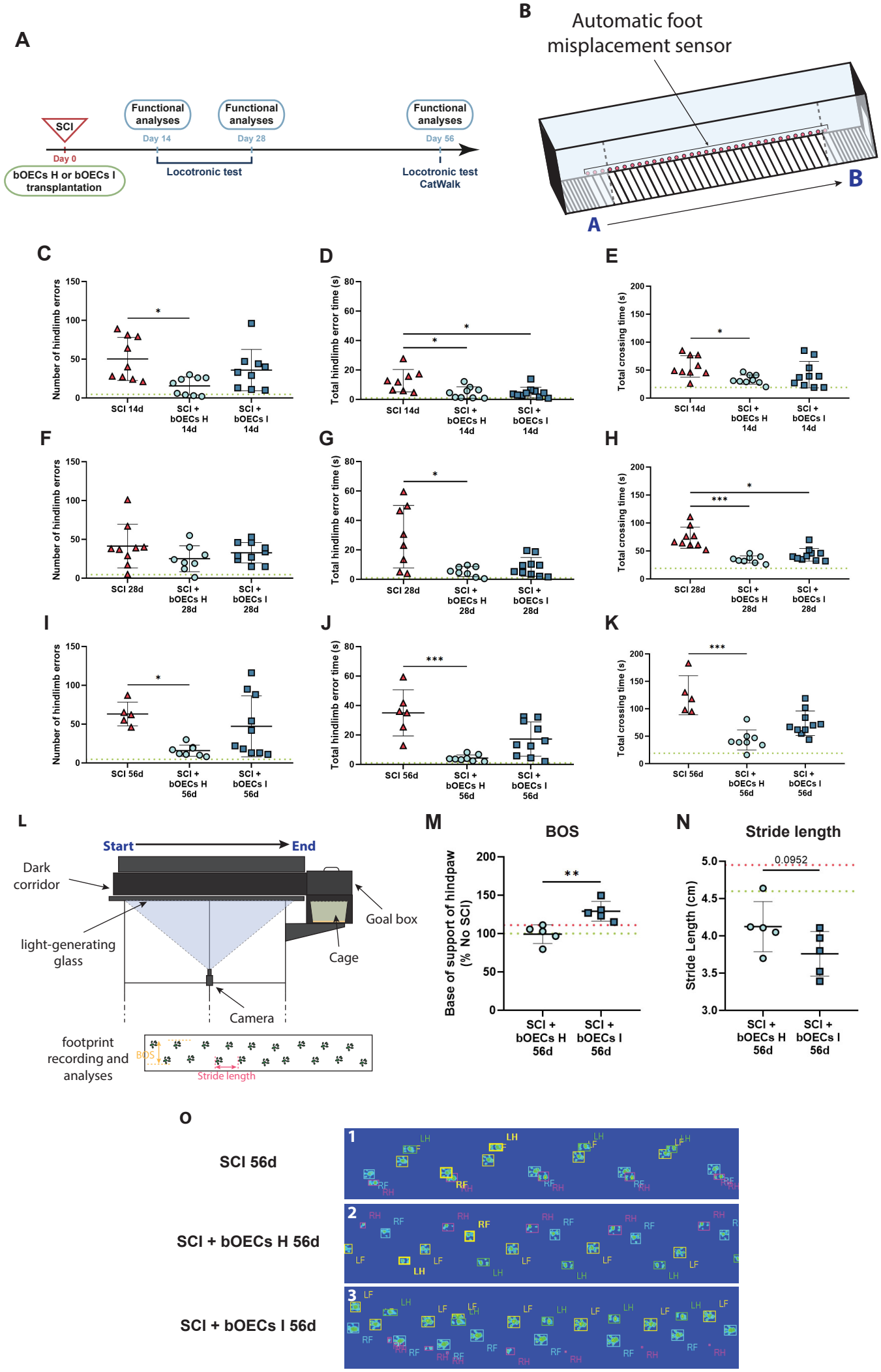
A
SCI
Day 0
bOECs H or bOECs I transplantation
Functional analyses
Day 14
Functional analyses
Day 28
Locotronic test
Functional analyses
Day 56
Locotronic test
CatWalk
B
Automatic foot misplacement sensor
A
B
C
Number of hindlimb errors
SCI 14d
SCI + bOECs H 14d
SCI + bOECs I 14d
D
Total hindlimb error time (s)
E
Total crossing time (s)
F
SCI 28d
SCI + bOECs H 28d
SCI + bOECs I 28d
G
H
I
SCI 56d
SCI + bOECs H 56d
SCI + bOECs I 56d
J
K
L
Start
End
Dark corridor
light-generating glass
Goal box
Cage
Camera
footprint recording and analyses
BOS
Stride length
M
BOS
Base of support of hindpaw (% No SCI)
N
Stride length
Stride Length (cm)
0.0952
O
SCI 56d
SCI + bOECs H 56d
SCI + bOECs I 56d

Fig 5:

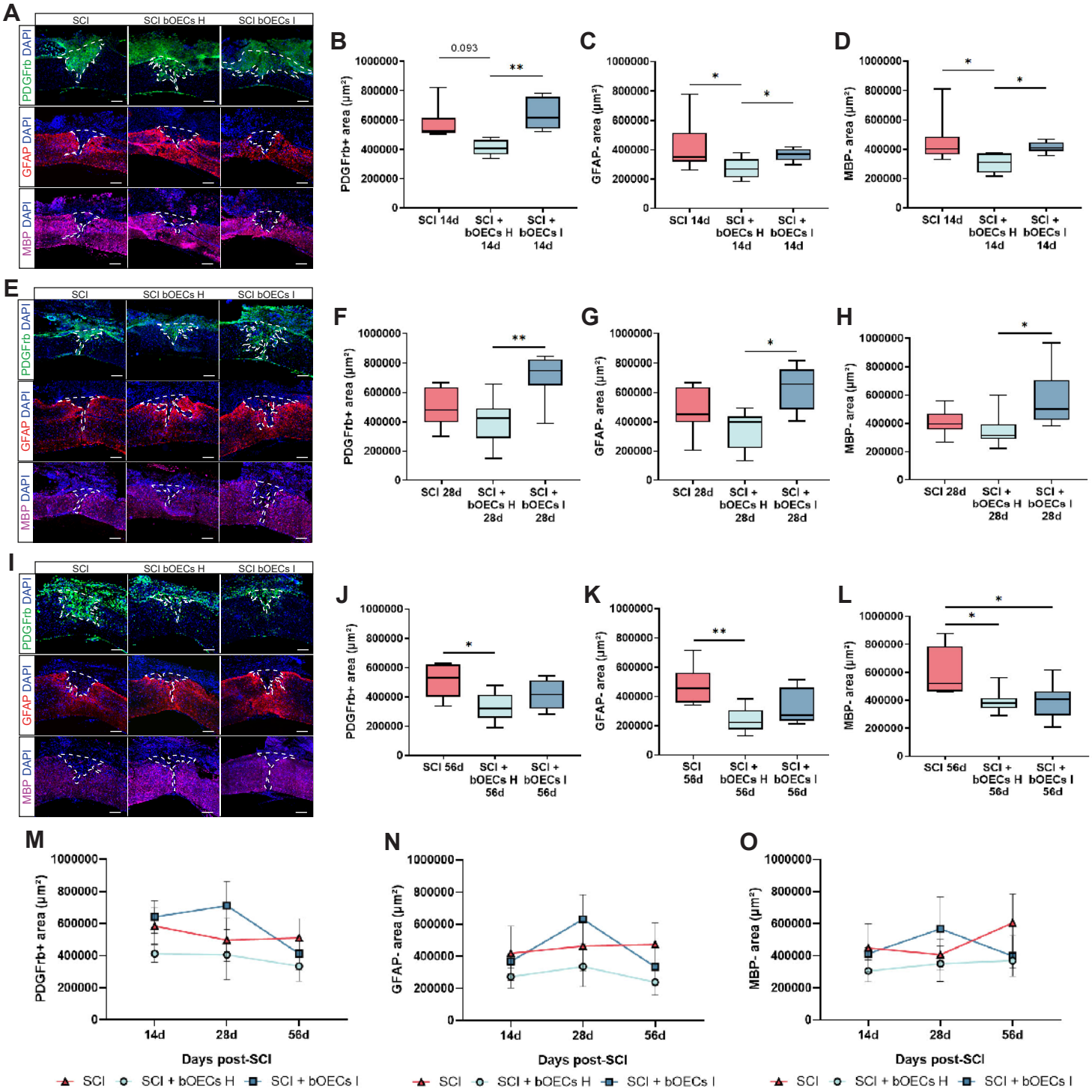
A
SCI
SCI bOECs H
SCI bOECs I
PDGFrb DAPI
GFAP DAPI
MBP DAPI
B
0.093
**
PDGFrb+ area (µm²)
SCI 14d
SCI + bOECs H 14d
SCI + bOECs I 14d
C
*
*
GFAP- area (µm²)
D
*
*
MBP- area (µm²)
E
F
**
SCI 28d
SCI + bOECs H 28d
SCI + bOECs I 28d
G
*
H
*
I
J
*
SCI 56d
SCI + bOECs H 56d
SCI + bOECs I 56d
K
**
L
*
*
M
N
O
14d
28d
56d
Days post-SCI
SCI
SCI + bOECs H
SCI + bOECs I

Fig 6:

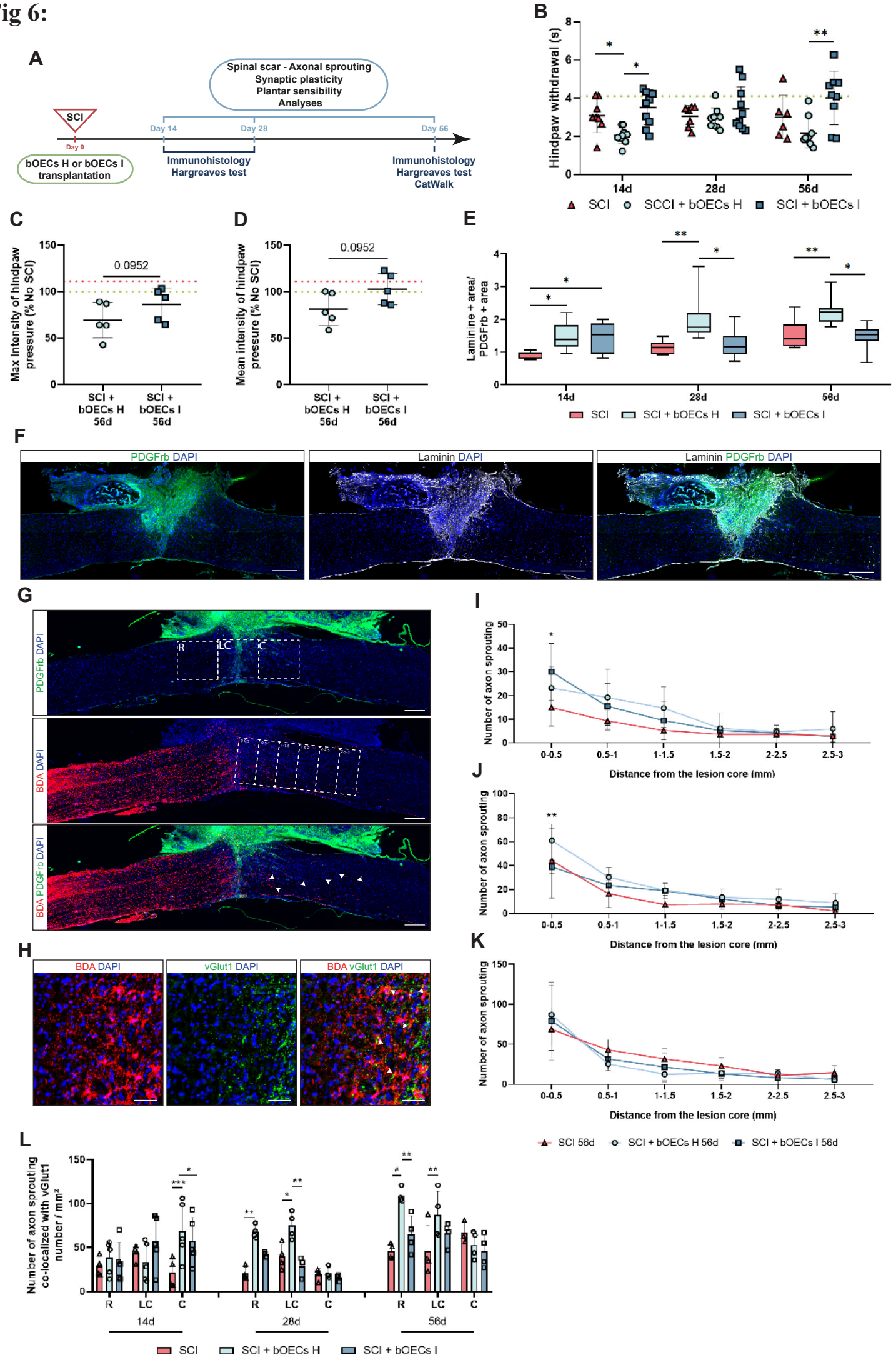
A
Spinal scar - Axonal sprouting
Synaptic plasticity
Plantar sensibility
Analyses
SCI
Day 0
Day 14
Day 28
Day 56
bOECs H or bOECs I transplantation
Immunohistology
Hargreaves test
Immunohistology
Hargreaves test
CatWalk
B
Hindpaw withdrawal (s)
14d
28d
56d
SCI
SCCI + bOECs H
SCI + bOECs I
C
Max Intensity of hindpaw pressure (% No SCI)
0.0952
SCI + bOECs H 56d
SCI + bOECs I 56d
D
Mean intensity of hindpaw pressure (% No SCI)
0.0952
E
Laminine + area/ PDGFrb + area
14d
28d
56d
SCI
SCI + bOECs H
SCI + bOECs I
F
PDGFrb DAPI
Laminin DAPI
Laminin PDGFrb DAPI
G
PDGFrb DAPI
BDA DAPI
BDA PDGFrb DAPI
R
LC
C
H
BDA DAPI
vGlut1 DAPI
BDA vGlut1 DAPI
I
Number of axon sprouting
Distance from the lesion core (mm)
J
Number of axon sprouting
Distance from the lesion core (mm)
K
Number of axon sprouting
Distance from the lesion core (mm)
SCI 56d
SCI + bOECs H 56d
SCI + bOECs I 56d
L
Number of axon sprouting co-localized with vGlut1 number / mm²
R
LC
C
14d
28d
56d
SCI
SCI + bOECs H
SCI + bOECs I

Fig 7:

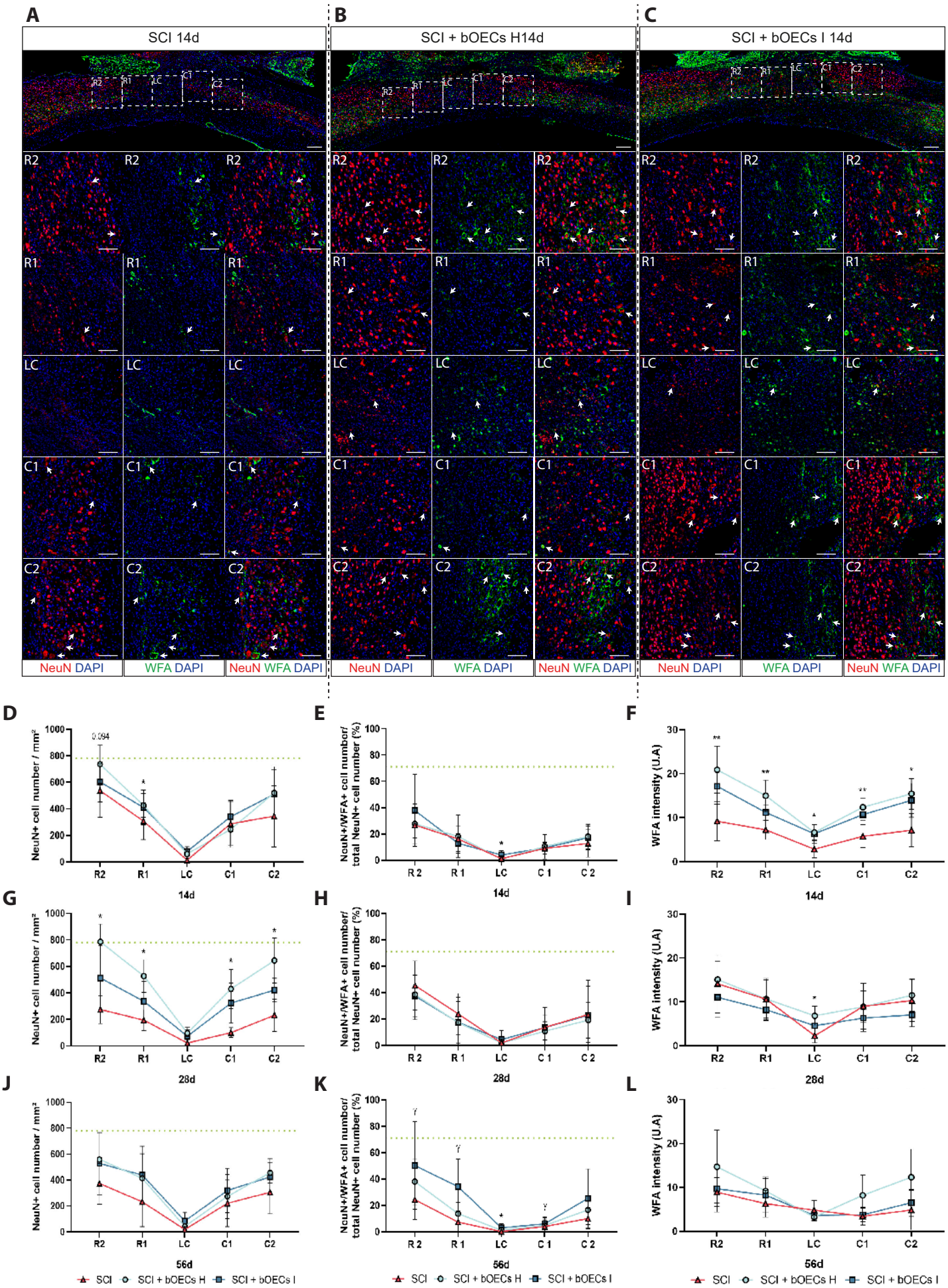
A
SCI 14d
B
SCI + bOECs H14d
C
SCI + bOECs I 14d
R2
R1
LC
C1
C2
NeuN DAPI
WFA DAPI
NeuN WFA DAPI
D
E
F
G
H
I
J
K
L
NeuN+ cell number / mm²
NeuN+/WFA+ cell number/ total NeuN+ cell number (%)
WFA intensity (U.A)
14d
28d
56d
SCI
SCI + bOECs H
SCI + bOECs I

Fig 8:

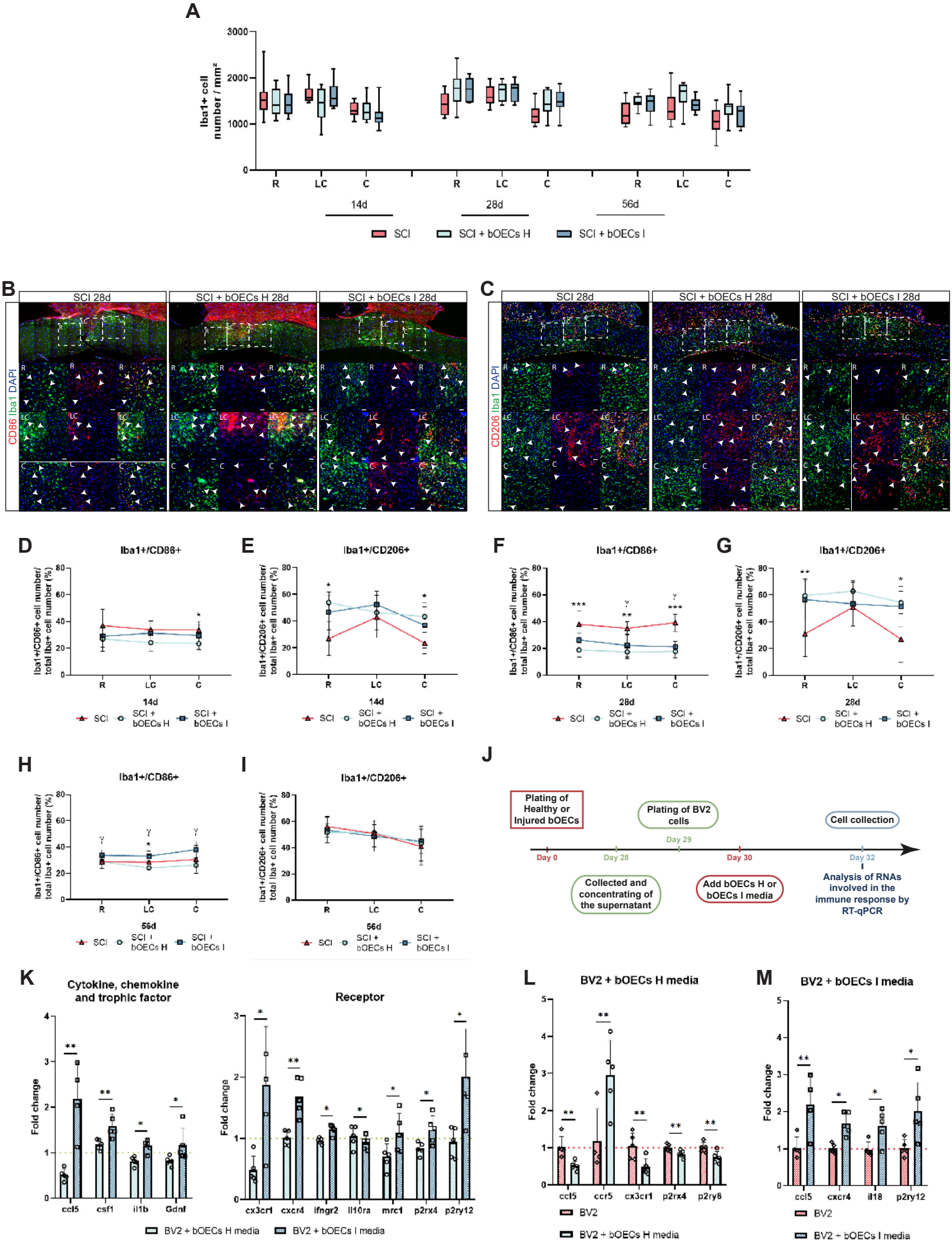
A
Iba1+ cell number / mm²
R
LC
C
14d
28d
56d
SCI
SCI + bOECs H
SCI + bOECs I
B
SCI 28d
SCI + bOECs H 28d
SCI + bOECs I 28d
CD86 Iba1 DAPI
C
CD206 Iba1 DAPI
D
Iba1+/CD86+
E
Iba1+/CD206+
F
Iba1+/CD86+
G
Iba1+/CD206+
H
Iba1+/CD86+
I
Iba1+/CD206+
J
Plating of Healthy or Injured bOECs
Plating of BV2 cells
Cell collection
Day 0
Day 28
Day 29
Day 30
Day 32
Collected and concentrating of the supernatant
Add bOECs H or bOECs I media
Analysis of RNAs involved in the immune response by RT-qPCR
K
Cytokine, chemokine and trophic factor
Receptor
Fold change
ccl5
csf1
il1b
Gdnf
cx3cr1
cxcr4
Ifngr2
Il10ra
mrc1
p2rx4
p2ry12
BV2 + bOECs H media
BV2 + bOECs I media
L
BV2 + bOECs H media
ccl5
ccr5
cx3cr1
p2rx4
p2ry6
BV2
M
BV2 + bOECs I media
ccl5
cxcr4
il18
p2ry12